Theor Chem Acc (1997) 97:14–40

Theoretical
Chemistry Accounts
© Springer-Verlag 1997

Direct SCF direct static-exchange calculations of electronic spectra

Hans Ågren[1], **Vincenzo Carravetta**[2], **Olav Vahtras**[1], **Lars G.M. Pettersson**[3]

[1] Institute of Physics and Measurement Technology, Linköping University, S-58183, Linköping, Sweden
[2] ICQEM-C.N.R., Via Risorgimento 35, I-56100 Pisa, Italy
[3] FYSIKUM, University of Stockholm, Box 6730, S-113 85 Stockholm, Sweden

Received: 28 December 1996 / Accepted: 8 April 1997

Abstract. Applications of the direct SCF direct static-exchange method are reviewed for three different types of systems (free molecules, polymers, and surface adsorbates) and for six types of spectroscopy (X-ray absorption-, -emission-, and -shake-up spectroscopy, ultraviolet photoelectron emission, X-ray Raman and circular dichroism spectroscopy.

Key words: Direct methods – Excited states – Oligomers – Adsorbates – X-ray spectra

1 Introduction

The experimental progress made in determining spectra and properties of large molecular aggregates of technological interest has represented a great challenge as regards concomitant development of methods for quantum simulations. The implementation of the direct SCF technique (DSCF) by Almlöf and coworkers in 1982 [1] served as the start for one such branch of development and significantly broadened the possibility of systematic modeling using the Hartree-Fock method and the associated independent particle interpretation. The focus on the SCF method was related to its qualitatively correct description of the electronic structure of closed-shell systems. The applications of the direct atomic orbital SCF, or integral-direct SCF, techniques have since then diversified to include calculations on a broad range of extended systems and macromolecules, and apart from total energies and electronic structures of closed-shell systems, such calculations now include many features like energy gradients and structure optimization, static and dynamic response properties and various types of spectra [2–6].

Using the DSCF approach for spectra and property calculations it has been possible to eliminate the same type of bottlenecks as for electronic structure calculations, namely the calculation, storage, retrieval, and possibly also the transformation, of two-electron integrals. As in the direct generation of SCF wave functions one has to resort to direct handling of atomic orbital integrals and compute them as they are needed in order to obtain calculations that are CPU limited instead of limited by the available disk storage.

In the calculation of spectra the canonical Hartree-Fock orbitals and eigenvalues obtained from the DSCF wave function itself form a starting point that at least for some types of electronic spectra is a reasonable approximation. A variant thereof is the "direct ΔSCF" method in which two separate (direct) SCF calculations are performed and used to compute the energy and the matrix element for an electronic transition. Two extensions may be considered within the DSCF technology and which encompass a great number of spectroscopies; namely, time-dependent Hartree-Fock and improved virtual orbital Hartree-Fock, also known under the synonyms the random phase approximation (RPA) and the static exchange approximation (STEX), respectively.

The RPA method based on DSCF wave functions has been developed to quite an advanced stage using both integral direct and matrix direct techniques in solving the RPA equations and can now be applied to a great number of linear and non-linear properties and spectra [4, 5, 7, 8]. However, RPA is limited to excitations of electrons from outer shells only, due to incomplete handling of relaxation of highly excited states. This limitation to the low-energy part of the electronic spectrum is unfortunate in light of the remarkable improvements in resolution and quality of synchrotron excitation techniques generating tunable, monochromatized, radiation also in the high-energy X-ray region. Although the STEX technique can be viewed as an approximation to RPA, it has some inherent advantages in this respect, since it is also applicable to core excitations in the X-ray region for which the RPA method thus has fundamental problems. Some years ago it became clear to us that it would be desirable to broaden the scope of the STEX method and include DSCF technology in order to obtain applicability to large species, and to

Correspondence to: H. Ågren

achieve a development similar to that of direct RPA. It is the intention with the present work to review the direct STEX method and its applications and results to date.

2 Method and calculations

Several accurate ab initio methods adopting basis set projection are now available for the calculation of molecular excited electronic states. The conventional approaches are based on the, more or less straightforward, extension to excited states of techniques for the calculation of accurate ground state energies and wave functions (CI, MCSCF, MBPT, CC, etc). Other techniques are based on the use of Green's function or propagator techniques or on the closely related response function technique and have the significant advantage of directly computing excitation energies and transition probabilities, and properties of excited states. These approaches are able to give accurate results taking into account, more or less extensively, the electron correlation. However, all of them are in practice limited, by intrinsic and numerical problems in the corresponding computational algorithms, to the description of either small systems and/or of a restricted number of excited states in the spectrum. If the interest is in the description of the electronic spectrum over a large energy range, covering for instance both the discrete and the continuum states, or if the spectrum of interest is at very high energy involving excitation/ionization of the inner core electrons, we have to resort to less sophisticated ab initio methods that can offer a simplified but more complete view of the electronic excitation processes. These simpler approaches are also the only ones that can be practically employed for large molecular systems where the computational effort of the more accurate techniques is prohibitive.

2.1 Basic approximation levels for photoabsorption

The STEX approximation is a simple independent channel approach that can be considered physically well-suited to describe core electron excitations in molecules for reasons that we will discuss in detail in the following. Recently, we presented [6] a direct implementation of the STEX method within the framework of the direct SCF program DISCO of Almlöf and coworkers [1]; by avoiding any storage and retrieval of integrals, the algorithm can be efficiently used for large molecular species and very large basis sets. It may be appropriate, at this point, to compare the STEX approximation to other approaches, more commonly applied to the valence shell electrons, that can also be employed for the calculation of the full excitation spectrum.

2.1.1 The random phase approximation

In the RPA [9] also known as time-dependent Hartree-Fock, the excited electronic states are defined through excitation operators having the following form

$$\hat{\mathbf{T}}_I^\dagger = \sum_{j,\mu} (\mathbf{X}_{j\mu,I}\, \hat{a}_\mu^\dagger \hat{a}_j + \mathbf{Y}_{j\mu,I}\, \hat{a}_j^\dagger \hat{a}_\mu) \ , \tag{1}$$

where the indices j and μ run over the occupied and virtual SCF orbitals, respectively, of the ground state. The coefficients $\mathbf{X}$ and $\mathbf{Y}$ are determined by the RPA equation

$$\begin{pmatrix} \mathbf{M} & \mathbf{Q} \\ \mathbf{Q}^* & \mathbf{M}^* \end{pmatrix} \begin{pmatrix} \mathbf{X}_{.,I} \\ \mathbf{Y}_{.,I} \end{pmatrix} = \omega_I \begin{pmatrix} \mathbf{I} & \mathbf{0} \\ \mathbf{0} & -\mathbf{I} \end{pmatrix} \begin{pmatrix} \mathbf{X}_{.,I} \\ \mathbf{Y}_{.,I} \end{pmatrix} \ , \tag{2}$$

with

$$\mathbf{M}_{lv,j\mu} = \delta_{lj}\delta_{v\mu}(\epsilon_\mu - \epsilon_j) + (1 - \delta_{lj})(2[vl|\mu j] - [jl|\mu v]) \tag{3}$$

$$\mathbf{Q}_{lv,j\mu} = (2[vl|\mu j] - [\mu l|vj]) \ . \tag{4}$$

It can easily be shown that RPA corresponds to the linear response of the ground state SCF wave function. If the set of excited states generated by the promotion of an electron from the fixed occupied orbital j is considered to define the "excitation/ionization channel" j, we can see that the RPA excitation operator in Eq. (1) involves coupling of different channels. Because of the presence of the $\mathbf{Y}$ component in Eq. (1) the RPA excitation operator corresponds to something more than a simple mixing of singly excited states. These "de-excitation terms" are often regarded as introducing some electron correlation in RPA (corresponding to first order in the "fluctuation" potential). They are certainly responsible for a convenient feature of the method, i.e. the gauge invariance of the computed excitation probability, or oscillator strengths, within the limits of a complete basis set.

Due to the relative "compactness" of the RPA equation [the matrix in Eq. (2) has dimension equal to twice the product of the number of occupied and virtual orbitals], this approach has been largely applied to medium-size molecules; the range of applications significantly widened by the introduction of matrix direct [10] and integral direct algorithms [4, 7]. UV spectra and photoionization cross sections [11] and in general linear response properties [10] due to the excitation of the valence-shell electrons can be obtained with reasonable accuracy. Shape resonances as well as Feshbach resonances, due to the embedding of discrete excited states of a closed channel in the continuum of one or more open channels, can also be described due to the inclusion of the channel coupling in the RPA equation. However, because of the projection on "frozen" orbitals of the ground state, RPA cannot handle properly the effect of the electron relaxation for the highly excited states. Spectroscopies, such as NEXAFS (near edge X-ray absorption fine structure), shake-up/off and XES (X-ray emission), which involve excitations of the core shell electrons by electron impact or absorption/emission of X-rays can thus not be described quantitatively. The RPA excitation energies are for such processes several eVs away from the experimental results and the intensities can also be strongly affected by neglecting the electron relaxation around the core-hole [12], as is the case with the RPA approach.

2.1.2 The Tamm-Dancoff approximation

In the Tamm-Dancoff approximation (TDA) the term **Y** of Eq. (1) is dropped, so that the excitation operator reduces to

$$\hat{\mathbf{T}}_I^\dagger = \sum_{j,\mu} (\mathbf{X}_{j\mu,I}\ \hat{a}_\mu^\dagger \hat{a}_j)\ . \tag{5}$$

The representation of the excited state as a linear combination of single-particle excitations has the advantage of decreasing the computational effort, since the dimensionality of the projected TDA equation is half that of the RPA equation. The effect on the computed excitation energies is usually rather small but the TDA intensities are no longer gauge invariant, even within the limits of basis set completeness, and this evidently complicates the comparison of computed and experimental spectra. This inconvenience is not sufficiently balanced by the limited gain in the numerical resolution of the TDA equation and, as a matter of fact, this approximation has been applied only in a limited number of test cases. TDA anyway constitutes the simplest model for the description of channel interaction. This effect can be of importance for obtaining quantitatively accurate intensities for UV and UPS spectra of molecules where several valence excitation channels can be active in a relatively small energy range.

2.1.3 The static-exchange approximation

We can obtain a substantial reduction of the computational effort by neglecting the channel coupling in Eq. (5) so that the excitation operator takes the expression

$$\hat{\mathbf{T}}_I^\dagger = \sum_{\mu} (\mathbf{X}_{j\mu,I}\ \hat{a}_\mu^\dagger \hat{a}_j) = \sum_{\mu} (\mathbf{X}_{j\mu,I}\ \hat{a}_\mu^\dagger) \hat{a}_j\ . \tag{6}$$

This independent channel approach can be considered as a low-level approximation for the valence shell, but it is physically well justified for processes involving core electron excitations because of the large energy separation of core levels of different atomic species and the generally large spatial separation of core orbitals on different atoms. Moreover, the independent channel single-excitation approach can be easily implemented in terms of relaxed occupied orbitals optimized for the specific (core-hole) channel considered. The configuration interaction implied by Eq. (6) can in fact be easily converted to the solution of a one-electron problem for the excited electron in the static potential of the remaining molecular ion, such that the spin of the total system is preserved, i.e. that exchange interaction is accounted for. This static-exchange approach is, for the reasons just outlined, the one we choose for the study of processes involving the excitation/de-excitation of core electrons in large molecular systems.

The calculation of the final states is thus divided into the following steps:

1. The fully relaxed core-hole state is obtained by an SCF optimization.
2. The STEX Hamiltonian is constructed from the core-hole state orbitals such that the total spin of the initial state is preserved when the excited electron is included.
3. The excited state orbital is generated as a virtual orbital from diagonalizing the STEX Hamiltonian with the occupied core-hole state orbitals projected out; the excited state orbitals are thus orthonormal with respect to the relaxed core-hole orbitals.

Consider, for example, a molecule with a closed-shell ground state. The core-hole state is obtained by an SCF optimization. These relaxed orbitals together with the virtual orbitals from the STEX Hamiltonian are used to build the final singlet state,

$$|\Psi_{j\epsilon}\rangle = \frac{1}{\sqrt{2}} (a_{\epsilon_\alpha}^+ a_{j_\alpha} + a_{\epsilon_\beta}^+ a_{j_\beta}) |\Psi_{\text{ref}}\rangle\ , \tag{7}$$

where a_j annihilates one electron in the chosen core orbital φ_j and a_ϵ^+ creates one electron in a virtual orbital φ_ϵ which may be a bound or a continuum orbital orthogonal to the occupied orbitals of the reference (closed-shell) state $|\Psi_{\text{ref}}\rangle$ obtained for double occupancy of the relaxed orbitals. The total energy of the final state is, by virtue of the ordinary Slater-Condon rules, expressed in the molecular orbital basis as

$$E = \sum_{i \neq j,\epsilon} (h_{ii} + F_{ii}^{\text{cs}}) + F_{jj}^{\text{cs}} + F_{\epsilon\epsilon}^{\text{cs}} + (jj|\epsilon\epsilon) + (j\epsilon|\epsilon j)\ , \tag{8}$$

where h is the one-electron Hamiltonian and F^{cs} is the Fock operator associated with the remaining closed-shell orbitals

$$F^{\text{cs}} = h + \sum_{i \neq j,\epsilon} 2J_i - K_i\ . \tag{9}$$

The final step, the optimization of the excited orbital φ_ϵ, can be perceived in terms of the functional derivative of the energy with respect to this orbital

$$\frac{\delta E}{\delta \varphi_\epsilon} = 0 \tag{10}$$

which gives a traditional Hartree-Fock equation for the excited orbital,

$$F^j \varphi_\epsilon = \epsilon \varphi_\epsilon\ , \tag{11}$$

where F^j is a modified Fock operator,

$$F^j = h + \sum_{i \neq j} (2J_i - K_i) + J_j + K_j\ , \tag{12}$$

also called the static-exchange Hamiltonian. The eigenvalue problem of Eq. (11) is solved by projection on a basis set orthogonalized to the occupied orbitals.

The static-exchange Hamiltonian can be constructed in an atomic orbital (AO) basis with traditional direct SCF techniques if the correction to the traditional Fock operator is transferred to the density matrices. Rewriting Eq. (12) in terms of a closed-shell Fock operator, we have

$$F^j = F - J_j + 2K_j\ , \tag{13}$$

which has an AO representation

$$F^j_{ab} = F_{ab} - (jj|ab) + 2(aj|jb) \tag{14}$$

$$= h_{ab} + \sum_{cd}(2(ab|cd)D^C_{cd} - (ad|cb)D^X_{cd}) \ , \tag{15}$$

where we have introduced the modified Coulomb and exchange densities [6]

$$D^C_{ab} = D_{ab} - \frac{1}{2}c_{aj}c_{bj} \tag{16}$$

$$D^X_{ab} = D_{ab} - 2c_{aj}c_{bj} \ . \tag{17}$$

This modification can easily be implemented in any direct SCF code, thereby utilizing the efficiency of density screening, non-Abelian symmetry, parallelism, etc, to construct the static-exchange Hamiltonian and the computational work will be equivalent to one direct SCF iteration.

In general, the ground state may be an open-shell state, in which case the static-exchange Hamiltonian may be written

$$F' = F - \sum_j \alpha_j J_j - \sum_j \beta_j K_j \ . \tag{18}$$

The spin-coupling coefficients α_j, β_j are derived from the final state energy expression, as in Eq. (8), and the modified densities in Eq. (17) will have the form [13]

$$D^C_{ab} = D_{ab} - \frac{1}{2}\sum_j \alpha_j c_{aj}c_{bj} \tag{19}$$

$$D^X_{ab} = D_{ab} + \sum_j \beta_j c_{aj}c_{bj} \ . \tag{20}$$

A standard basis set may be adequate for calculating the electronic structure of a molecule, but it is usually insufficient for highly excited states in the continuum and the static exchange Eq. (11) must thus be solved in an augmented basis set. In addition to a standard basis set used for the ground and core-hole states, we add a large (typically 19*s*19*p*19*d* functions) diffuse basis centered on the core site, allowing for a proper description of the Rydberg states and the continuum. This augmentation basis set is added only when solving the static-exchange equation, which substantially reduces the cost of the calculations.

The excitation energies ω_μ of the NEXAFS spectrum are obtained by adding the core ionization potential, obtained by the ΔSCF procedure, to the eigenvalues of the STEX matrix and the corresponding oscillator strengths f_μ are obtained from the dipole matrix elements (both in length and velocity gauges) between ground state and STEX final states. In the discrete part of the spectrum the eigenpairs of excitation energies and oscillator strengths provide a true spectral representation, while in the continuum they may provide a primitive spectrum for a Stieltjes imaging (SI) procedure [14, 15]. This is a moment theory approach by which a primitive spectrum ω_μ, f_μ of order N is converted to a quadrature spectrum of order $n (n \ll N)$ such that the first $2n$ spectral moments

$$S(-2k) = \sum_\mu (\omega)^{-2k}_\mu f_\mu \tag{21}$$

are reproduced. Here the oscillator strength (length gauge) is written in terms of the excitation energy and the transition dipole moment as

$$f_\mu = \frac{2}{3}\omega_\mu |\langle \Psi_0 | \ \vec{r} \ | \Psi_{j\mu} \rangle|^2 \ . \tag{22}$$

The dipole transition amplitude is calculated with both the initial and final states projected onto the augmented basis set. Since the initial and final state orbitals have been optimized separately and thus are non-orthogonal, we must compute explicitly the cofactors or use a corresponding orbitals technique like that introduced by Amos and Hall [16] and later generalized by Malmqvist [17]. From the quadrature spectrum Stieltjes derivatives and the final Stieltjes imaged NEXAFS integrated cross sections are obtained as described in Ref. [14].

2.2 The STEX approximation to the shake phenomenon

The static-exchange description of the shake phenomenon [18] has much in common with that of NEXAFS. A major difference is that there are two electrons participating in the process, one primary photoelectron excited to the continuum, and one secondary "shake" electron, which is excited to discrete (shake-up) or continuous (shake-off) levels, the energies and intensities of which constitute the shake spectrum. As for NEXAFS, we ignore fine structure and effects due to vibronic coupling, angular distributions, or finite lifetimes, etc., which in principle can be incorporated in the STEX analysis of shake spectra, but which are not essential to the main features of the method. The first assumption made in deriving the STEX formulas for shake-up concerns the primary photoionization process itself, namely the use of the "sudden approximation", which in turn includes the strong-orthogonality condition for the outgoing photoelectron, neglect of the so-called conjugate and hole-mixing terms and also of the variation of the photoelectron matrix elements with photon energy. Further approximations refer to the treatment of electron correlation of the initial and final states, rather than the process itself. A discussion of the role of these approximation schemes for the analysis of shake-up (models and computations) can be found in Refs. [19, 20].

Using these approximations the basic entity to compute is the generalized overlap amplitude

$$G_i = \left\langle \Psi^{N-1}_f | \hat{a}_x | \Psi^N_{gs} \right\rangle , \tag{23}$$

where Ψ^N_{gs} and Ψ^{N-1}_f are the ground state and the final ionic state wave functions, respectively, and $\hat{a}_x$ is the annihilation operator for the ground state core orbital φ_x. As for NEXAFS, the STEX method implements a "scattering view" rather than a "state-by-state view" to the shake phenomenon, i.e. it treats one channel completely (full intrachannel interaction and basis set expansion). In the STEX approximation for the shake effect the shaked electron interacts with an $N-2$ electron potential rather than an $N-1$ potential as in NEXAFS. Within this approximation, we thus assume that a shake-up/shake-off state is expressed as

$$\Psi_f^{N-1} = \Psi_{xj}^{N-2} \otimes \phi_\epsilon \,, \tag{24}$$

where the secondary shake-up/off electron function ϕ_ϵ is strongly orthogonal to the remainder N-2 electron state Ψ_{xj}^{N-2} and determined variationally in the field of the fully relaxed but frozen two-hole (core orbital x, valence orbital j) ion:

$$F^{xj}\phi_\epsilon = \epsilon\phi_\epsilon \,. \tag{25}$$

We construct one static-exchange Hamiltonian F^{xj} for each shake-channel defined by the primary ionization orbital x, by the secondary ionization (or excitation) orbital j and by the particular spin coupling S. For a closed-shell ground state and non-degenerate orbitals x and j, the static-exchange Hamiltonian has the following general expression

$$F^{xjS} = F + \alpha_x J_x + \beta_x K_x + \alpha_j J_j + \beta_j K_j \,, \tag{26}$$

where the coupling coefficients α, β depend on the adopted coupling scheme [21]. The molecular orbitals building up this static-exchange Hamiltonian are obtained by an optimization for the x:th hole. If there are open shells in the ground state the correction to the closed shell Fock operator is obtained by adding $\hat{J}$ and $\hat{K}$ operators in Eq. (26) corresponding to these open shells. A useful approximation for the "passive" open shells is the high spin approximation, which can be accommodated here by a summation with additional coupling coefficients $\alpha = -1, \beta = 1/2$, neglecting the spin coupling of these open shells with the orbitals x and j.

The excitation energies of the shake spectrum are obtained by adding the second ionization potential (shake-off threshold), for each given shake channel $IP_{xjS}^{N-2} = E_{xjS}^{N-2} - E_{gS}^{N}$, to the eigenvalues of the STEX matrix, while the corresponding transition moments are obtained as monopole matrix elements between ground state and STEX final states projected on mutually non-orthogonal sets of molecular orbitals. For the discrete part the sets of pairs of excitation energies and overlap amplitudes form a true representation of shake-up energies and intensities, respectively, while in the continuum each pair forms a primitive excitation energy and intensity factor for the continuum part. The shake-off profile can be obtained in full correspondence with the NEXAFS case, considering overlap amplitudes rather than oscillator strengths in the Stieltjes imaging procedure [18].

The spin-coupling coefficients in Eq. (26) can readily be derived from expectation values of the $(N-1)$ electron Hamiltonian over the open-shell configuration state functions (CSF), i.e. least linear combination of determinants that fulfil spin and spatial symmetry (monopole selection rule) for the final state, using the standard Slater-Condon rules. Each ordered spin-coupling sequence defines a CSF with a specific energy and a specific STEX Hamiltonian. The coupling order matters since CSFs obtained by different coupling orders are interacting over the Hamiltonian. Two spin-coupling schemes, out of the three possible ones to couple the three open-shell orbitals [core, valence and virtual (STEX) orbitals] to a doublet state, have been considered in the shake-up as well as in the NEXAFS calculations. Both schemes generate two linearly independent final doublet states, corresponding to singlet or triplet intermediate coupling, respectively. In the first scheme ("holes" coupling) the core and the valence orbitals are coupled first to singlet or triplet and then the coupling to the virtual orbital is considered; in the second scheme ("excitation" coupling) we couple first the valence and the virtual orbitals (again to singlet or triplet) and then the core orbital. In certain cases the "excitation" coupling can be motivated, e.g. when the virtual orbital has a strong valence character; however the "hole" coupling is generally the most reasonable one. In the STEX approximation the sum of intensities for the two coupling orders has the same value. In general the "singlet" and "triplet" shake channels are interacting and the coupling of these two channels would be the first most natural extension of the STEX approach.

2.3 SCF approximation for X-ray emission

In the case of non-resonant XES, where we assume that the emitting sample is isotropic and thus independent of the nature of the preparation process, the transition rate for spontaneous emission is given by

$$I \propto \omega^3 |\langle \Psi_i | V | \Psi_f \rangle|^2 \,, \tag{27}$$

where ω is the transition frequency and V represents the electron-photon interaction, normally in the electric dipole approximation. In this case the initial state Ψ_i is a core-hole state corresponding to a chosen core orbital and the final state Ψ_f is an arbitrary valence hole state. In Sect. 2.1.3 we derived the static-exchange approximation for the final states in the absorption process. In the emission process a similar approximation is practical, even though the number of final states is considerably smaller. We assume that the final state can approximately be described by ground state orbitals, since the valence hole relaxation effects are an order of magnitude smaller than the orbital relaxation effects associated with the core-hole state. In this way we obtain all possible final states in a single calculation.

The transition matrix elements to be calculated over separately optimized initial and final states involve two sets of mutually non-orthogonal orbitals. Following Malmqvist [17], the transition overlap matrix is given by

$$\mathbf{X}_{ab}^{if} = \langle \varphi_a^i | \varphi_b^f \rangle \,, \tag{28}$$

where $\varphi^{i(f)}$ denotes the orbital set associated with the initial (final) state. The objective is to find a transformation that brings $\mathbf{X}^{if}$ to diagonal form in such a way that the inactive orbitals of each set are transformed among themselves only, and that the transformation of the active orbitals may be supported by the CI expansion. The method applies to a large class of CI expansions. In our case, where the point of departure is a closed-shell SCF state, the only active orbitals (in the sense of CI) are the two orbitals that are active in the transition. Partitioning of Eq. (28) into inactive (I) and active (T) blocks,

$$\mathbf{X}^{if} = \begin{pmatrix} \mathbf{X}^{if}_{\mathrm{II}} & \mathbf{X}^{if}_{\mathrm{IT}} \\ \mathbf{X}^{if}_{\mathrm{TI}} & \mathbf{X}^{if}_{\mathrm{TT}} \end{pmatrix} \tag{29}$$

the corresponding orbital method may be summarized by the transformation

$$\mathbf{C}^{i} = \begin{pmatrix} \mathbf{U}^{i}_{\mathrm{I}} & -(\mathbf{X}^{if}_{\mathrm{TI}}\mathbf{X}^{if^{-1}}_{\mathrm{II}})^{\dagger}\mathbf{U}^{i}_{\mathrm{T}} \\ 0 & \mathbf{U}^{i}_{\mathrm{T}} \end{pmatrix} \tag{30}$$

$$\mathbf{C}^{f} = \begin{pmatrix} \mathbf{U}^{f}_{\mathrm{I}} & -\mathbf{X}^{if}_{\mathrm{TI}}\mathbf{X}^{if^{-1}}_{\mathrm{II}}\mathbf{U}^{f}_{\mathrm{T}} \\ 0 & \mathbf{U}^{f}_{\mathrm{T}} \end{pmatrix} , \tag{31}$$

where the $\mathbf{U}$ are unitary matrices that act within the inactive or active subspaces and are defined through the singular value decompositions

$$\mathbf{U}^{i\,\dagger}_{\mathrm{T}}\mathbf{X}^{if}_{\mathrm{II}}\mathbf{U}^{f}_{\mathrm{I}} = \mathbf{D}_{\mathrm{I}} \tag{32}$$

$$\mathbf{U}^{i\,\dagger}_{\mathrm{T}}\left(\mathbf{X}^{if}_{\mathrm{TT}} - \mathbf{X}^{if}_{\mathrm{TI}}\mathbf{X}^{if^{-1}}_{\mathrm{II}}\mathbf{X}^{if}_{\mathrm{IT}}\right)\mathbf{U}^{f}_{\mathrm{T}} = \mathbf{D}_{\mathrm{T}} , \tag{33}$$

where $\mathbf{D}_{\mathrm{I}}$ and $\mathbf{D}_{\mathrm{T}}$ are diagonal matrices. The final step to obtain fully biorthonormal orbitals involves the scaling of one of the transformed orbital sets, say the final state orbitals, with the inverse of the corresponding diagonal element in Eq. (32) or (33), and to scale the CI coefficients with all diagonal elements to the power of the orbital occupancy in the corresponding determinant.

2.4 Cluster models

The chemisorption site at the metal surface is described using a cluster model which consists of a limited number of atoms (up to 50 atoms have been used in the reviewed applications); the bulk structure and positions are maintained for all cluster atoms and only the adsorbate structure and chemisorption site have been optimized. For the geometry optimizations the density functional (DFT) program deMon [22, 23] is used in conjunction with functionals including gradient corrections. The atoms interacting directly with the adsorbate are described, without further approximations, at the all-electron level using the "SDZC" basis set of Tatewaki and Huzinaga [24], extended with two diffuse *p*-functions and one additional diffuse *d*-function. For the more distant, next-nearest and farther neighbors a simplified description using the one-electron effective core potential (ECP) model developed by Wahlgren and coworkers [25] is used. In this approach the core, including the 3*d* shell, is described by a static potential, which includes the effects of relaxation and polarization of the 3*d* orbitals, but only treats explicitly the 4*sp* valence electrons. The basis set used is a (4*s*1*p*) primitive basis contracted to [2*slp*] [25]. This description has been extensively tested and used in a number of chemisorption studies [26].

3 Applications of the direct SCF direct static-exchange method

The direct SCF techniques for core-electron spectroscopies allow spectra to be generated using a description close to the basis set limit for smaller gas-phase molecules and allow the study of two important classes of problems in the field of X-ray spectroscopy: surface adsorbates and polymers. Both of these are in principle infinitely extended systems that can be treated using either a fully periodical approach (where the one- or two-dimensional translational symmetry is explicitly used) or a cluster or oligomer approach in the cases of surface adsorbates and polymers, respectively. The first approach refers to band theory applications for systems with periodic boundary conditions and to extensions thereof to defect band theory or super-cell methods for studying spectra with localized excitations (excitons). In the present work we will describe applications based on the second type of approach, where the effect on a (basically) localized excitation of the surrounding is given by a cluster model or a part of the polymer. With this approach one considers a sequence of clusters (oligomers) that models the full bulk (polymer), and studies the convergence of a property or a spectrum within this sequence. One thus attempts to find the limiting behavior by successive enlargements of the cluster models, and studies the smallest repeat unit up to a cluster of such a large size that it can be considered to represent the infinite system. These two approaches have different relative merits and limitations and often give quite complementary interpretations.

One advantage with the cluster (oligomer) approach is that it allows for an easy decomposition of spectra into local contributions and, in the case of polymers, gives an interpretation in terms of building blocks. It can, however, be computationally demanding and requires size-extensive methods that must also be applicable for larger systems, i.e. with an appropriate scaling of the computational effort with the system size. The RPA method mentioned in the preceding section is an example of such a method. The static-exchange method is a strict approximation to RPA, but has the above-mentioned advantage of being applicable to core excitations and to provide an easy representation of partial channel cross sections. It is scalable towards extended species by means of the integral-direct and basis set augmentation algorithms [5] and by implementing ECP, as mentioned in the previous section. The direct SCF direct STEX method has so far been applied to three types of systems: to free molecules including molecules with functional groups, to polymers, and to surface adsorbates, and to six types of spectroscopic processes: X-ray absorption, -emission, and -shake-up spectroscopy, and ultraviolet photoelectron emission, X-ray Raman and circular dichroism spectroscopy. It is our intention with this work to briefly review these applications.

3.1 X-ray absorption spectra

3.1.1. Free molecules

CO exhibits a few salient NEXAFS features around the onset of the ionization potential that are quite characteristic for many other small molecules and that serve as a good test for the STEX technique: a very strong

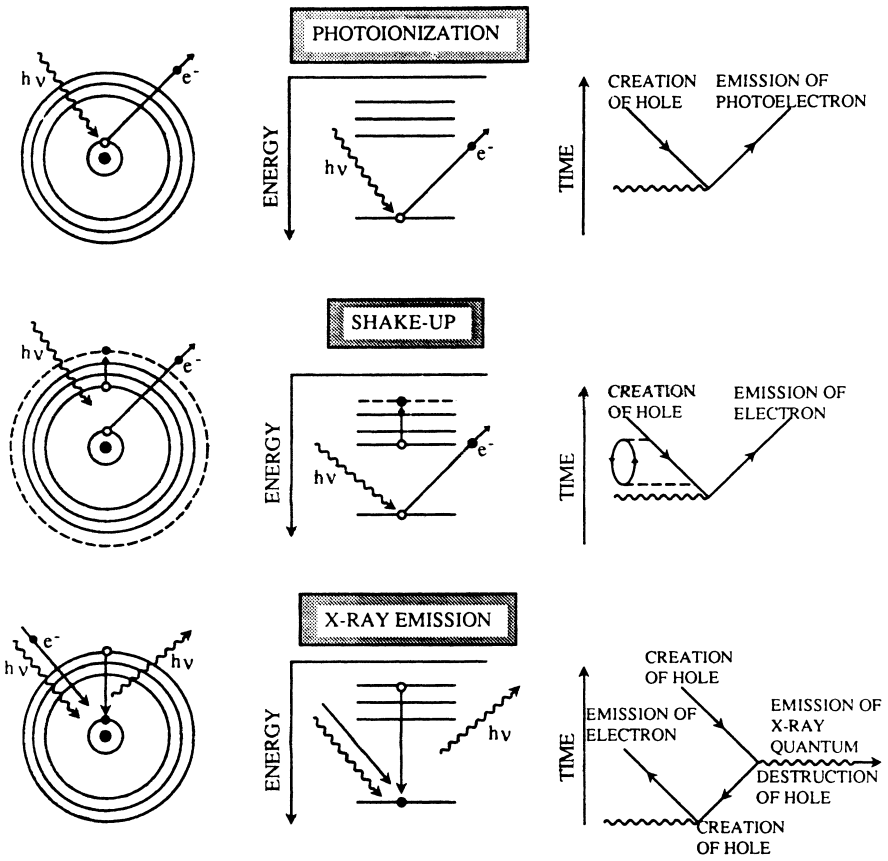

Fig. 1. Some of the phenomena simulated by the STEX technique as pictorially represented by the Bohr model, by one-electron diagrams and by many-body diagrams

Table 1. Energies (eV) and oscillator strengths for C1*s* and O1*s* core excitations in free CO. From Ref. [41]

Transition	E^a_{exp}	E^b	E^c	E^d	O^b	O^c	E^d	$\langle r^2\rangle^e$
C1*s*		289.01	0	289.36 (0)	0.1082	0.2707	0.1362[f]	22.60
2π	287.31	5.61	4.85	293.96 (4.6)	0.0038	0.0157	0.0030	61.03
$3s\sigma$	5.14	8.39	5.79	294.86 (5.50)	0.0038	0.0610	0.0062	73.46
$3p\pi$	6.12	8.01	5.89	294.95 (5.59)	0.0016	0.001	0.0004	79.17
$3p\sigma$		8.86	6.92	295.78 (6.42)	0.0006	0.0011	0.0001	227.49
$4s\sigma$	7.49	9.72	7.30	295.89 (6.53)	0.0002	0.0034	0	
$3d\pi$		9.67	7.40	295.97 (6.61)	0	0.0001	0.0005	
$4p\sigma$								
O1*s*								
2π	534.11	535.93	0	535.04 (0)	0.0507	0.0579	0.0580	27.39
$3s\sigma$	4.69	4.77	3.86	538.68 (3.64)	0.0002	0.0002	0.0009	56.09
$3p\pi$	5.67	5.81	4.82	539.63 (4.59)	0.0001	0.0001	0.0001	82.56
$3p\sigma$		6.14	4.90	539.65 (4.61)	0.0001	0	0	
$4s\sigma$	6.79	7.09	6.20	540.45 (5.41)	0.0001	0	0	
$3d\pi$		7.43	6.65	540.55 (5.51)	0.0013	0.0005	0	
$4p\sigma$		7.61	6.95	540.66 (5.63)	0.0001	0.0001	0.0003	

[a] Ref. [79]
[b] Ref. [80]
[c] Ref. [81]
[d] STEX Ref. [41]
[e] Expectation value of $\hat{r}^2$ operator over excited orbital [41]
[f] Experiment: 0.167 ± 0.02 (Ref. [82])

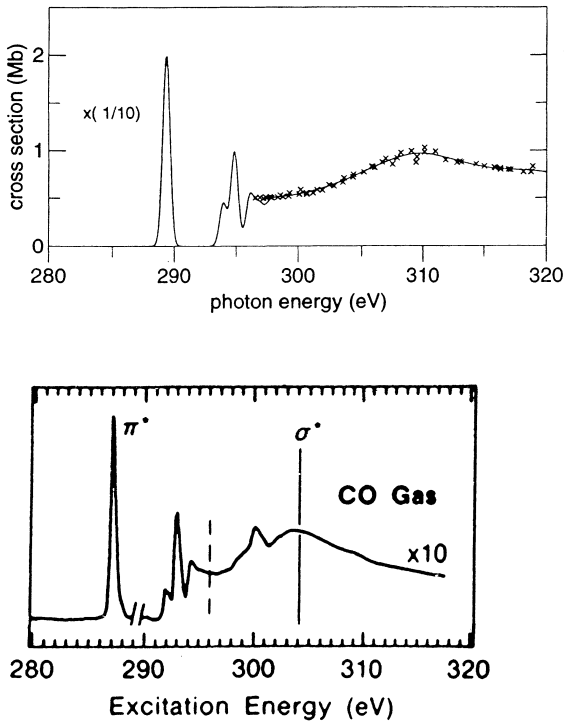

Fig. 2. C1*s* NEXAFS spectrum for gas phase CO from STEX calculations [41] and from experiments [83]

discrete $1s \rightarrow \pi^*$ resonance, a weak remainder of a Rydberg progression converging to the ionization limit, a shape resonance in the σ channel above the ionization limit, and (many-electron) fine structure superposed on the near-edge continuum. The features of the experimental carbon and oxygen NEXAFS spectra are well-reproduced by the STEX calculations.

When the term values are computed relative to the ionization potential a quite good agreement results: within 1 eV for absolute term values and within a few tenths of an eV for relative term values (Table 1). Since the STEX energies by construction relate to the ionization potentials, these determine to a large extent the absolute shifts of the STEX spectrum (C1*s* ionization in CO turns out to be a particularly difficult case, as investigated in some detail in Ref. [27]). Screening relaxation is neglected in the STEX procedure (i.e. the change in relaxation of bound electrons due to the presence of the excited electron), which explains the push-up in energy for the valence-like π^* level. (For a limited number of valence levels the extra relaxation energy can be computed using ΔSCF calculations.) On the other hand, the screening relaxation is negligible for Rydberg levels (as inferred from spectator autoionization experiments on CO [28]) and the energetics of the Rydberg levels are well reproduced. Because the σ^* shape resonance is also valence-like, it is pushed to somewhat higher energies, just as is the discrete π^* resonance. NEXAFS spectra of open-shell molecules are intrinsically more complicated; an illustration of that is given by a recent STEX open-shell calculation of molecular oxygen [29].

3.1.2 Polymers

As with other theoretical methods, applications of the STEX method have the dual roles of providing proper assignments of the spectra and to investigate the validity of simplified analyzing tools which can be used for property-to-structure relationships. In X-ray absorption one such tool is given by the building block principle, which states that the spectrum of the full compound can be understood as a sum of the spectra of its constituting subunits. The decomposition of a spectrum into contributions from its constituents (the building blocks) can be accomplished by comparisons with spectra from analogous molecules which differ by one or two functional groups. The simplest building block is the diatom, the bonding of which determines the position of both discrete and continuous resonances (often being of π^* and σ^* type for organic π-electron systems), and in the most basic version of the building block principle the NEXAFS spectrum is given as a superposition of diatomic spectra [30].

Since the experimental spectra often superpone the X-ray absorption from chemically shifted species pertaining to a given kind of atom, a building block decomposition can be difficult to carry through in practice. An alternative way to proceed is to assemble building blocks to the composite molecule, where the building blocks can be in the form of a free molecule or a functional group in an environment where the building block unit presumably is little perturbed. This can be the case for even quite complicated repeat units, but the model can also break down even for quite simple organic molecules, as for some π-conjugated systems [30, 31]. On purely experimental grounds it can evidently be difficult to determine when this is the case. Theory gives a way out here, because it can separate the different core-sited spectra for atoms of the same kind, and also because it can systematically investigate the perturbation of each building block on any other building block and follow the convergence of added building block spectra to the spectrum of the full polymer repeat unit.

The direct STEX technique has proven to be particularly rewarding for building block analysis, owing to the inherent "high resolution" of the method, especially in the discrete part of the NEXAFS spectra. A recent study of poly(ethylene terephthalate) (PET) and poly(bisphenol-A-carbonate) (PC) compounds serves as a good example of this contention [32]. The STEX technique could here provide correct assignments and offered the possibility of studying the formation of the spectra from the single building blocks to the full polymer repeat unit, and thereby to set the limit for the building block model for these compounds. Figure 3 shows how the carbon PET spectrum is subdivided into contributions from the phenyl connecting and unconnecting carbons, from the carbonyl group and from the hydrocarbon chain.

Another analyzing tool in NEXAFS which can be studied by STEX simulations is the bond-length-with-ruler principle, which relates the position of resonances to the bond lengths. We refer to Ref. [30] for this particular aspect. Yet another promising aspect of

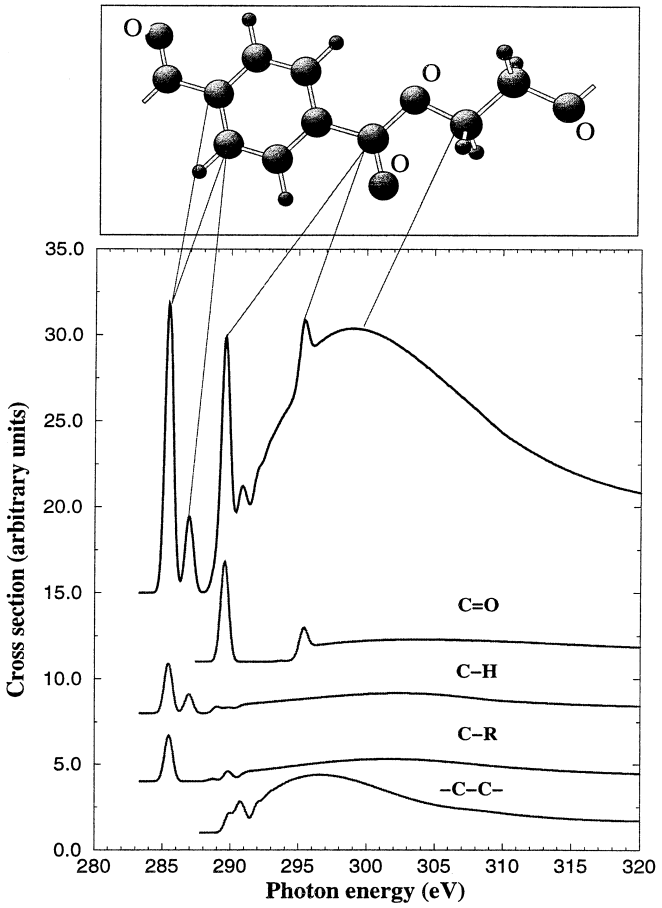

Fig. 3. The disintegration of the C1*s* and O1*s* NEXAFS spectra of poly(ethylene-terephthalate) in terms of building blocks. From Ref. [32]

STEX applications to NEXAFS refers to the capability for orientational probing. This capability stems from the possibility of using polarized X-ray photons with high intensity and energy resolution, implying that individual states can be excited selectively by switching polarization directions and/or tuning the excitation frequency. From the experimental point of view one needs very simple situations, e.g. π-electron systems with separated π- and σ manifolds, i.e. when the spectral depletion in one or the other symmetry is accomplished by just switching the *E*-vector in orthogonal directions. In more common situations with complex spectra the orientational probing relies on a proper assignment of states in the NEXAFS spectra, and simulations are required for symmetry assignments of the core-excited states and for determination of oscillator strength components in the different polarization directions. A good example of this is given by the recent study [33] of the NEXAFS spectra of thin fluon films, where the orientation of the polymer

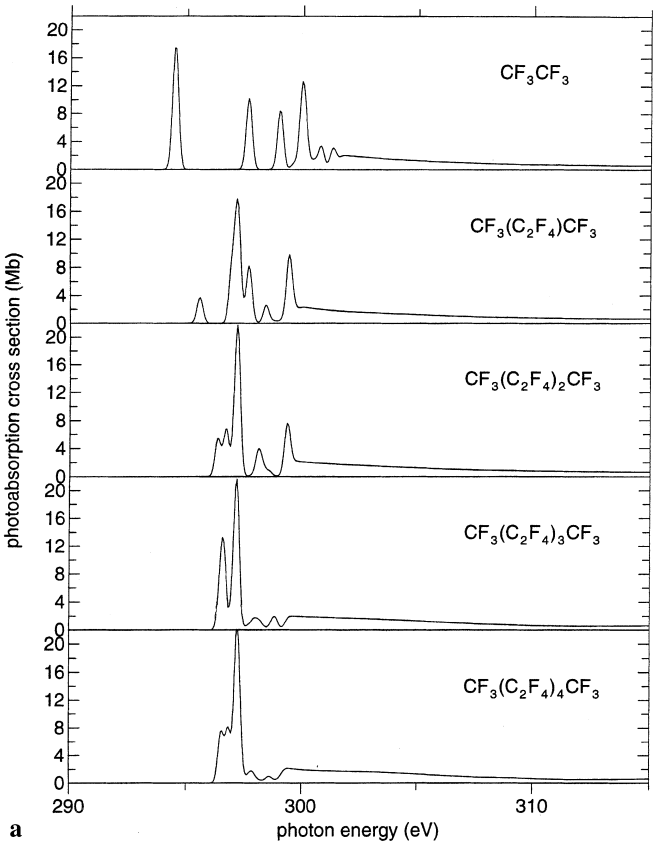

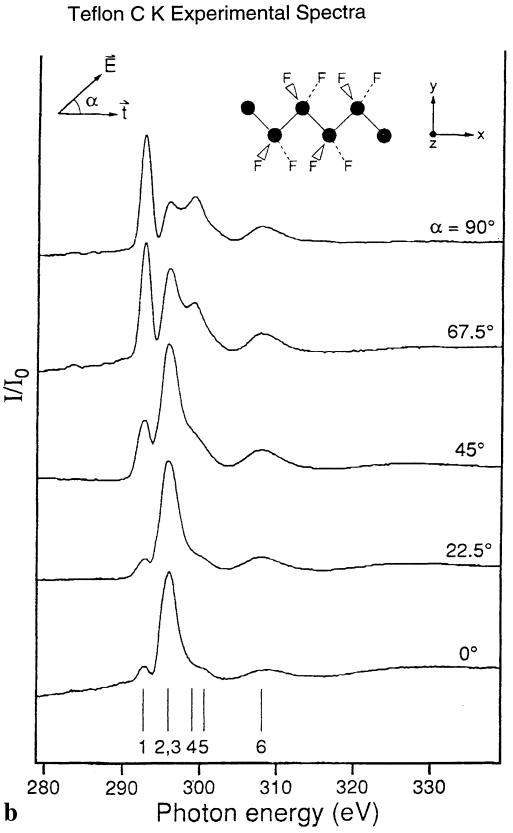

Fig. 4. a Simulated C K-edge NEXAFS spectra of the mid-atom in $CF_3(C_2F_4)_{n-1}$ CF_3, $n = 1, 2, 3, 4, 5$. The three first peaks in the *bottom panel* correspond (from *left* to *right*) to *z*, *y* and *x* polarized X-ray absorption, respectively. From Ref. [33]. **b** Experimental C K-edge NEXAFS spectra of poly-tetrafluoroethylene obtained by Ziegler et al. [84]. A definition of coordinates axes and polarization angle is found at the top of the figure

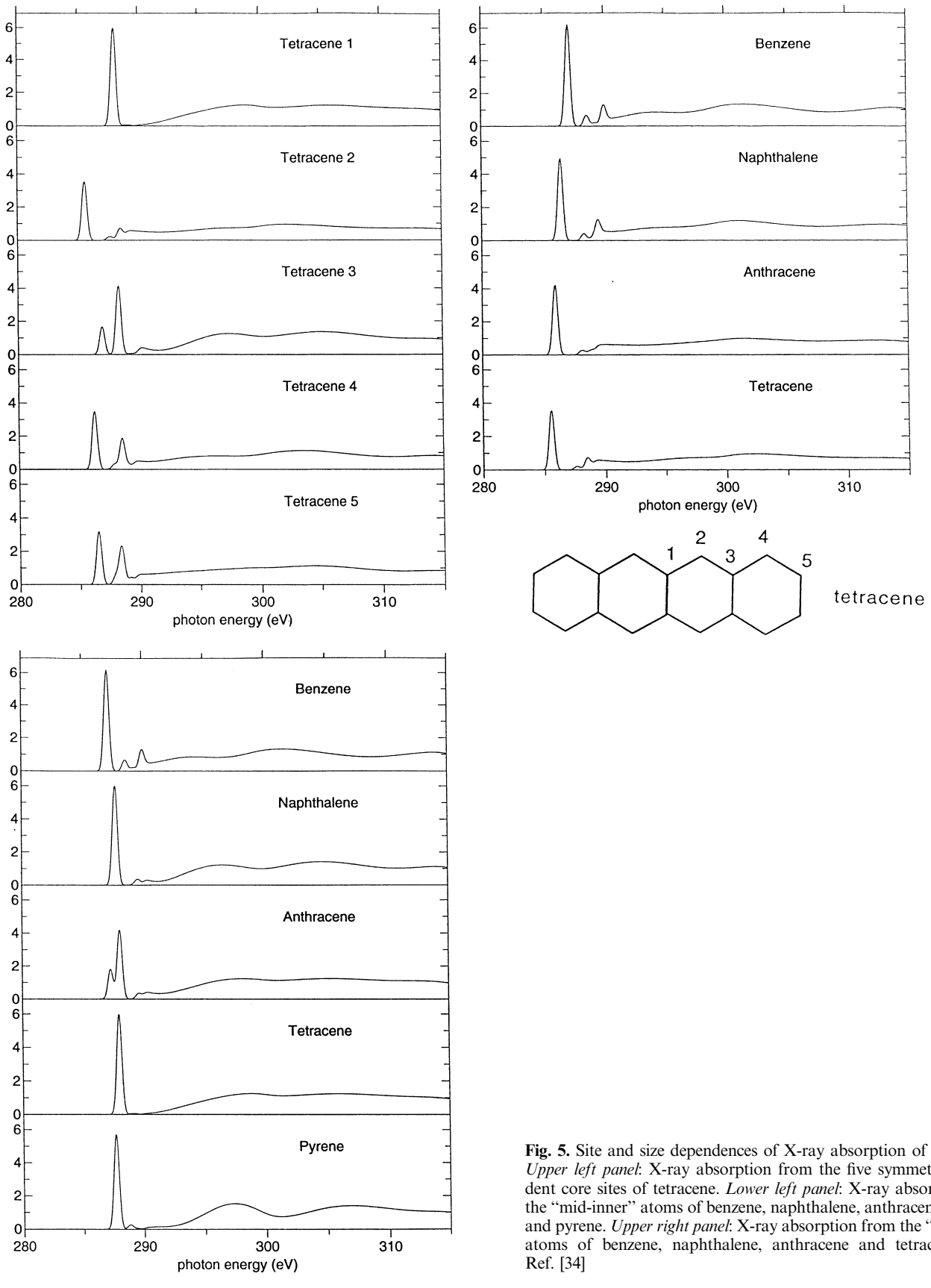

Fig. 5. Site and size dependences of X-ray absorption of polyacenes. *Upper left panel*: X-ray absorption from the five symmetry-independent core sites of tetracene. *Lower left panel*: X-ray absorption from the "mid-inner" atoms of benzene, naphthalene, anthracene, tetracene and pyrene. *Upper right panel*: X-ray absorption from the "mid-outer" atoms of benzene, naphthalene, anthracene and tetracene. From Ref. [34]

when slid onto the surface could be determined through STEX calculations comparing them with the experimental spectra.

The spectra were computed for x, y and z polarized E-vectors and, compared with the NEXAFS spectrum for the particular sample preparation, one could conclude that the poly-tetrafluoroethylene thin film is highly ordered, that the zig-zag structure prevails over the helical structure and that the polymer chain is directed along the assumed slide direction. It was also (less firmly) indicated that the carbon back plane is oriented orthogonal to the substrate surface. This illustrates well which type of conclusions we can anticipate from the application of the direct STEX technique in conjunction with NEXAFS measurements on oriented polymers. Related investigations on other polymeric systems can be found in Refs. [6, 34, 35].

Yet another property of NEXAFS spectra of polymers that can readily be studied by the direct STEX techniques using oligomer modeling is the appearance of excitons. An exciton is traditionally defined as an electronic level which is pulled down below the conduction band by the core-hole and which then localizes to the site of the core-hole. In the exciton interpretation of X-ray spectra, the energy levels thus shift and relocalize according to the creation of each particular core-hole, while in the band theory (non-excitonic) interpretation the excited levels evolve according to the energy bands and density of states of the ground state. The information content of the X-ray spectra obviously depends on whether the spectrum is excitonic or not. From π-electron theory [36] the occurrence of excitons is governed by a localization parameter expressed as the ratio of the core-valence Coulomb interaction and the width of the conduction band (the unoccupied π band). The excitonic character will be system dependent, chemically (site-) dependent as well as size dependent. STEX calculations using polyenes and polyacenes as prototype systems illustrate these statements very well.

For the polyenes one finds that there is a strong reduction of intensity of the first resonance for atoms in all positions. The site dependence is alternant both for energies and intensities. This alternation effect is damped when moving to the center of the polyene. The calculations demonstrate that the decrease of the first π resonance intensity follows from a decrease of localization with the increase of the polyene length, and a quite substantial reduction of the integrated π/σ intensity ratio is predicted.

The polyacenes (fused benzene rings) also show interesting site and size dependences of their absorption spectra [34]. In contrast to the linear polyene series, the polyacene series shows a rapid build-up of π^* excitons, with constant energy and intensity, conforming with the notion that the first π^* resonance in pyrene and graphite is strongly excitonic [34, 37, 38]. The excitonic character is, however, different for the two symmetry non-related carbon atoms in the polyacene series. In contrast to the inner atom spectra, the outer atom spectra [34] show a smooth decay in intensity and excitation energy with respect to the size of the polyacene chain. Considering the nearly constant energy and intensity, the exciton for the inner atom seems already to be present for benzene and persists all the way to polyacene, pyrene and graphite [37, 38]. We find that the double peak feature in the spectra of the shorter polyacenes [39] is given by the chemical shifts of the inner and outer atoms and that only terminal atoms show multiple structures in the discrete part. Similar to what is found for the polyenes the site-dependent trends for the C1s - π^* excitations are alternant. However, in contrast to the polyenes, the polyacenes show the strongest alternation effect for the mid (bulk) atoms rather than for the terminal atoms. All these features have been predicted by direct STEX calculations, providing in each case new explanations for the relevant experiments.

3.1.3 Surface adsorbates

Molecules adsorbed or chemisorbed on surfaces, that is surface adsorbates, constitute another class of systems which is conveniently studied by means of synchrotron radiation. The study of core excitations of such systems is of interest for many reasons: e.g. to explore dynamics, local electronic structure and binding. NEXAFS intensities may probe initial state charge transfer and hybridization, energy positions probe the final state screening and role of the core-hole, and vibrational or dissociative broadening can give clues to the site of adsorption, etc., so there are indeed many features of surface adsorbate interactions that become relevant issues in STEX calculations of NEXAFS spectra. As for polymers, NEXAFS is most useful for orientational probing of surface adsorbed molecules. It then becomes desirable to assign symmetries and to obtain accurate oscillator strengths and directional oscillator strength components through computations.

Some of the above-mentioned aspects of NEXAFS spectra of surface adsorbates have been studied by means of STEX calculations using cluster models for the surface: OH/Cu(111) [40] and CO/Cu(100) [41]. Additional systems under study are N_2 on Cu(100) and Ni(100), atomic adsorbates (C, N, O) on Cu(100), small hydrocarbons (CH, CH_2, CH_3, C_2H_2, C_2H_4) on different low-index Cu surfaces, but also larger adsorbates such as formate, acetate and glycine on Cu(110). Here we will focus on the STEX results for OH/Cu(111) and CO/Cu(100) as model systems for these studies. The properties of particular interest for these systems refer to the general cluster convergence of the spectra, the role of charge transfer (internal and external) in different spectral regions, the sub-symmetry cross sections and population analysis, initial and final state rules, the role of open shells and spin-coupling, the reliability of the surface modeling (all-electron versus effective core potentials) and to gauge invariance and sum rules.

3.1.3.1 Binding. The two prototype systems, OH/Cu(111) and CO/Cu(100), represent different types of interactions leading to chemisorption that are manifested differently in the NEXAFS spectra. In particular, the CO molecule as adsorbate has also been of interest for experimental studies of several effects associated with the X-ray absorption process itself, while the OH radical

species rather has a role as an intermediate species in catalytic processes on the surface. (The OH species also serves as a model of the bonding of methoxy radicals to the surface [42].) The hydroxyl copper system forms a case where the chemisorption involves an almost complete acceptor charge transfer into an already partially occupied (π) level, resulting in a very ionic interaction. The more common unsaturated systems, like CO/Cu(100), studied by NEXAFS have both donor and acceptor bonds, most often involving the adsorbate HOMO (σ or π) and LUMO (π^*), respectively, with the latter giving the net contribution for the carbonyl systems [30]. Thus, in contrast to the adsorption of OH, the charge transfer in the carbonyl case involves an initially empty orbital (empty in free CO), with a balance between acceptor and donor charges. This level, π^*, is also responsible for the major features of both the carbon and oxygen NEXAFS spectra, in that it collects almost all the discrete state oscillator strength. The π^* level therefore becomes self-screening. From the fact that the same level determines both the screening and the spectrum, we can anticipate that the carbonyl systems may present a different pattern in the cluster convergence of the NEXAFS spectra than is the case for the hydroxyl radical adsorbates. Comparison of the adsorbate binding to Cu(111) at on-top, bridge and various hollow positions showed that the face-centered cubic three-fold hollow site was the energetically favored one in the OH case [42] (which is different from, for example, CO/Cu(100) for which on-top sites are preferred). As shown in Refs. [40, 42] the OH/Cu interaction is mainly determined by ionic contributions and by the strong acceptor charge transfer to the OH 1π open shell.

3.1.3.2 Cluster size convergence. A question that needs to be investigated is the convergence of the computed spectra with the size of the cluster models used. For ground state properties of the surface adsorbed system quite a lot of experience has by now been gathered on how to construct appropriate computational models to give reliable chemisorption energies [26], shifts in vibrational frequencies, structures, etc. However, rather little is known about the performance of the cluster approach for general electronic spectra. Since, for core-electron spectroscopies such as NEXAFS, the excitation takes place from a very strongly localized electronic state, it should be mostly influenced by the local environment of the absorbing site. Thus, a less crucial dependence on the size of the model can be expected and the results should rather be dependent on the fact that the cluster gives a local electronic structure that is representative for the surface and site one wishes to model.

The general cluster convergence for the CO/Cu(100) and OH/Cu(100) systems, for clusters ranging up to 50 atoms, was found to be satisfactory, although not complete. The special character of the strong metal to adsorbate charge transfer involving partially occupied (OH) and unoccupied (CO) orbitals has particular consequences for this convergence. Excitations to orbitals mainly localized on the adsorbate were found to be converged already with clusters representing only the nearest neighbors to the chemisorption site, while excitations into the unoccupied levels of the cluster were more slowly convergent and could be considered to show the development of the locally projected band structure. For each cluster model several different electronic states were considered, with rather minor effects on the resulting spectra, since the differences mainly involve changes in the occupation of the cluster. One exception was found in the case of CO chemisorption, where clusters with e^2 open-shell occupation (C_{4v} notation) were found to lead to overscreening of the core-hole state. Considering the lowest energy states, different many-open-shell configurations were encountered for different clusters, but nevertheless spectra with consistent trends were obtained from the series of enlarged clusters, particularly when excitations into the open shells were also taken into account. The cluster modeling of NEXAFS spectra for these surface adsorbates thus seems to be less cluster-size dependent than that which is encountered in, for example, adsorbate binding energy calculations, where, even for relatively large clusters, the

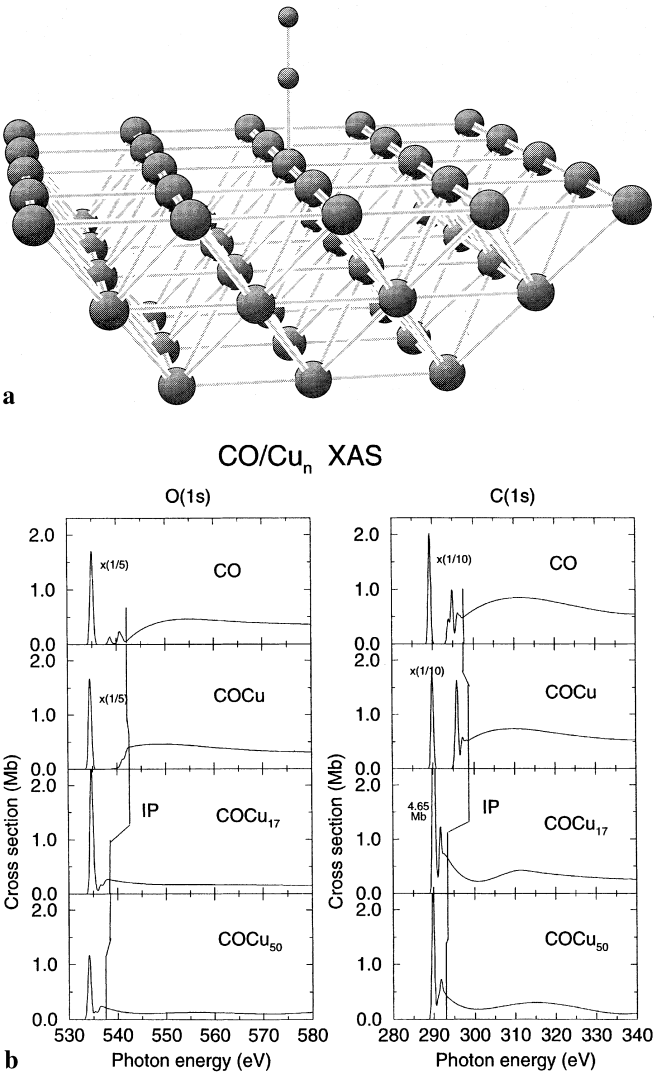

Fig. 6. **a** Structure of the $COCu_{50}$ cluster. CO is adsorbed with the carbon end. **b** O1*s* and C1*s* NEXAFS spectra for $COCu_n$; $n = 0, 1, 17, 50$ from STEX calculations [41]

finite cluster size can influence the computed binding energy and special techniques [43] need to be considered to improve the computational model.

3.1.3.3 Screening. For CO adsorbed on the copper surface the characteristics of NEXAFS spectra change in several ways common to both the carbon and the oxygen spectra: (1) loss of π^* intensity, (2) compression of the discrete spectrum, (3) lowering of the σ^* resonance and (4) vibrational broadenings and band broadenings of the C1s-π^* and O1s-π^* peaks. In chemisorbed CO the positions and strengths of both the discrete (π^*) and continuous (σ^*) resonances change due to the surface adsorbate interactions; the π^* mostly due to the charge transfer and 3d-π^* back-bonding. The σ^* is also affected since the extra screening population of the antibonding π^* in the ground state increases the CO bond length and therefore lowers the energy of this resonance.

The most salient difference observed between free and chemisorbed CO is thus the reduction of energy and intensity of the first π^* resonance and the compression of the discrete part of the spectrum. The compression can be seen as an effect of self-shielding, i.e. the constancy of the 1s-π^* excitation energy refers to that the π^* level is sufficiently localized to be self-screening [30]. Since the level, the π^* level, populated by screening and the level populated by the X-ray transitions is one and the same, the two processes are closely coupled for the intensive π^* NEXAFS spectra; the back-donation to the CO group is thus less effective for 1s excitation than for ionization, and the core excited state is less stabilized than the core-hole leading to the compression of the spectra. In a one-particle implementation, like the present STEX method, the potential is computed before the excitation, thus no more or less screening than that allowed by the bare core-hole state is obtained in the spectrum. Nevertheless, we can almost quantitatively predict the observed strong compression of the spectrum. In fact a reasonable interpretation of the compression of the discrete part of the spectrum can also be derived considering that, due to the presence of the surface, the screened core-hole is more diffuse than in the free molecule, the potential less attractive and, consequently, the energy range of the bound excited orbitals narrows.

3.1.3.4 Initial and final state rules. These are yet other aspects that have been addressed by STEX calculations [44]. The reduction of intensity for a core-excited state of a surface adsorbate is intimately connected to the question as to what degree the recorded X-ray signals reflect properties of the ground or the core state. Thus, according to the initial state rule, the NEXAFS intensity is reduced proportionally to the increase of the local atomic population in the ground state, thereby making connection to the character of the adsorbate bond and possibly also to the catalytic action of the surface.

The carbonyl-copper cluster data exhibit a strong variation of populations and intensities with cluster size. One finds covariation of the STEX oscillator strengths with both vacancy population (initial state rule) and excited state population (final state rule), but with the covariation of the final state population as the stronger. The STEX calculations thus give more support to a final state rule interpretation for oscillator strengths of surface-adsorbed species, and indicates that the decrease in π^* intensity going from free CO to CO/Cu(100) is primarily due to delocalization of the π^* orbital over the surface. These numbers thus confirm the delocalized character of the cluster π^* levels indicated by the small intensity and by the population numbers.

From the theoretical point of view it is relevant to note that the STEX potential is obtained from the fully relaxed core-hole state orbitals and that in the construction of the spectra by the STEX procedure the screening of the core-hole is separated from the population of the excited state through the interaction with the photon field. For self-screening levels like the π^* level, screening and population by excitation are correlated processes which to some extent calls for a multi-electron treatment. Ignoring the ''excitation'' one can expect the STEX procedure to overestimate the screening in the potential step, and therefore that it also overestimates the diffuseness (and underestimates the intensity) of the self-screening π^* orbital in the following excitation step.

3.2 X-ray emission spectra

XES is complementary to X-ray absorption, and relates more directly to the chemistry of the ground state species in that it probes the electronic structure for the occupied rather than the unoccupied levels. It shares with NEXAFS the property of being symmetry, orientational and polarization selective and that it reflects the local electronic structure of certain atomic symmetries. Unlike valence band photoemission for which one obtains signals that represent the delocalized states, the X-ray signal indeed reflects the part of the electronic structure that is localized to the site of the core electron, for instance localized to an adsorbate.

3.2.1 Free molecules

The carbon and oxygen XES spectra for free CO give a good illustration of the application to XES of the local selection model. Thus, transitions from the carbon ''lone-pair'' 5σ orbital are very intense in the carbon spectrum whereas transitions from the mostly oxygen-like 4σ orbital are strong in the oxygen spectrum. The delocalized 1π orbital is represented in both spectra, but, on a relative scale, more so in the oxygen spectrum in accordance with its p-population. These rules of thumb for one-center evaluations of X-ray intensities have been found adequate for spectra of a number of first- and second-row molecules, and provide simple means for interpretation [45, 46]. The inner valence 3σ orbital is one-center forbidden, and, subject to strong correlation breakdown [47] it is practically unobservable in XES [48].

CO thus illustrates that the simple molecular orbital interpretation of XES holds for the outer valence levels which are well described by one-particle MO (or quasi-particle) approximations; for first-row systems these levels are also the ones that provide strong intensity in

the spectrum. It is seen in Table 1 that the ΔSCF model works very well for the XES intensities when comparing with correlated calculations, and that the local population numbers give a good approximation of the full ΔSCF transition intensities.

3.2.2 Polymers

The direct SCF-ΔSCF techniques discussed in the present review have also been employed for non-resonant X-ray emission of polymeric compounds and fullerenes [49, 50]. For the latter compounds the direct SCF method, based on canonical Hartree-Fock orbitals (in the full symmetry point groups), reproduces the intensity profiles quite well. For polymers, like polyenes and polyacenes, the role of relaxation, and the accompanying exciton problem, has been analyzed in more depth [51, 52]. Direct ΔSCF calculations as well as π-electron theory have predicted the role of relaxation, and the associated exciton formation, for the interpretation of these spectra.

In some contrast to heterogeneous systems for which the role of relaxation is generally assumed to be fairly small, ΔSCF calculations predict a quite strong influence of relaxation on the spectral shape of X-ray emission of polyenes. In particular, the relaxation increases the intensity of X-ray emission from π levels in comparison with emission from σ levels, creating exciton-like features in the former part. The exciton character is site and size dependent; for longer polyenes it is stronger for mid- than for end-atoms and is found to be stronger at the top than at the bottom of the π band. The calculations predict a qualitatively different size dependency also for total X-ray emission intensities for mid- and end-atoms; an oscillatory damping for mid-atoms and a monotonous decrease for the end-atoms, which is reminiscent of the analogous behavior of the first π resonance in X-ray absorption spectra of polyenes. The direct ΔSCF calculations thus predict strong alternant site dependences when going from the end to the bulk of a polymer. The size dependence is connected to the strength of the core-valence interaction and excitons. The excitonic character can directly be related to a parameter defined as the ratio between the core-valence interaction and the width of a ''generalized'' π band. The latter encompasses the unoccupied π band and the occupied, emitting, level in question [52]. Thus the localization (exciton) parameter increases towards the top of the band.

A complication/simplification trend in going from small to large is obtained in relaxed as well as in frozen orbital calculations [53]; however, the simplified polymer spectra are predicted to be different in the two cases. The relaxation thus shifts intensity within the spectrum for each size and site, and introduces core-hole chemical shifts among the different sites, thereby scrambling the total spectrum. For the long chain limit one might still anticipate simplifications due to the marginal role of end atoms.

The ΔSCF calculations also indicate that conditions for exciton formation depend on several factors: on the process itself – the conditions for excitons are more favorable for X-ray emission than for X-ray absorption; on the system – polyacenes seem to be more favorable for excitons than polyenes; on the chemical environment – the excitons for the bottom atoms are stronger than for the top atoms in the spectra of the polyacenes.

3.2.3 Surface adsorbates

Despite the bulk sensitivity and low X-ray fluorescence yields inherent in the XES measurements, surface spectra of good quality have been produced by taking full advantage of the brightness of the modern synchrotron radiation sources [54–56]. CO adsorbed on a copper(100) surface was again used as the first critical test case for DISCO direct ΔSCF calculations of soft X-ray emission spectra of surface adsorbates. This also found motivation in the fact that the simplicity of the CO molecule with two core hole derived spectra has made it serve as a prototype for the remarkable features of molecular X-ray emission, with intensity in the two spectra closely following the degree of localization of the molecular orbitals on the different core sites [45, 47, 57].

Energies and intensities were obtained from separate state SCF wave functions and modeling the surface by clusters of copper atoms, up to $COCu_{50}$, using effective core potentials, as described in Sect. 3. The X-ray intensities were also evaluated from population analysis and from ground state frozen orbitals in order to test the validity of the local selection (one-center) and the initial

Table 2. Comparison of carbon and oxygen relative X-ray emission intensities of CO at different levels of approximations. Calculations not defined are SCF type calculations

Level Transition	GS[a] pop.	CS[a] pop.	Frozen[b] orbital	Relax[b] orbital	MCSCF[c]	CI[d]
$C1s^{-1}$-$5\sigma^{-1}$	0.78	0.64	1.11	0.82	0.949	0.850
$C1s^{-1}$-$1\pi^{-1}$	1.0	1.0	1.0	1.0	1.0	1.0
$C1s^{-1}$-$4\sigma^{-1}$	0.04	0	0.10	0.06	0.068	0.054
$C1s^{-1}$-$3\sigma^{-1}$	0.25	0.22	0.33	0.19		0.189[e]
$O1s^{-1}$-$5\sigma^{-1}$	0.05	0.04	0.10	0.09	0.079	0.074
$O1s^{-1}$-$1\pi^{-1}$	1.0	1.0	1.0	1.0	1.0	1.0
$O1s^{-1}$-$4\sigma^{-1}$	0.33	0.32	0.42	0.32	0.372	0.322
$O1s^{-1}$-$3\sigma^{-1}$	0.05	0.05	0.05	0.04		0.023[e]

[a] Population analysis [46]
[b] Ref. [58]
[c] Separate state MCSCF calculations [57]
[d] CI calculations with non-orthogonal molecular orbitals [47]
[e] Summed over four correlation split states [47]

and the final state rules. A first conclusion of this study was that calculations of spectra of surface adsorbates with the direct SCF direct ΔSCF approach do not present any greater difficulty than for free molecules. Thus a ΔSCF approach with small basis sets seems to constitute an equally good analyzing tool for surface XES as for XES, and is only limited by the number of atoms that can be treated in the cluster. Another conclusion drawn in Ref. [58] is that, except for the screening π^* level, all salient features of the XES spectra show rapid convergence with respect to cluster size. The small basis set dependency, taken together with fast convergence with cluster size, indicates good prospects for such calculations. On the other hand, the choice between the many possible electronic configurations of the clusters is not arbitrary. As in the corresponding NEXAFS case it is possible to find electronic configurations that give consistent local electronic structures, which well represent the surface and the site of the adsorbate and that also give consistent trends in the XES spectra. It seems to be more important to follow a series of clusters with similar ground state electronic configurations, rather than choosing the cluster with the lowest energy.

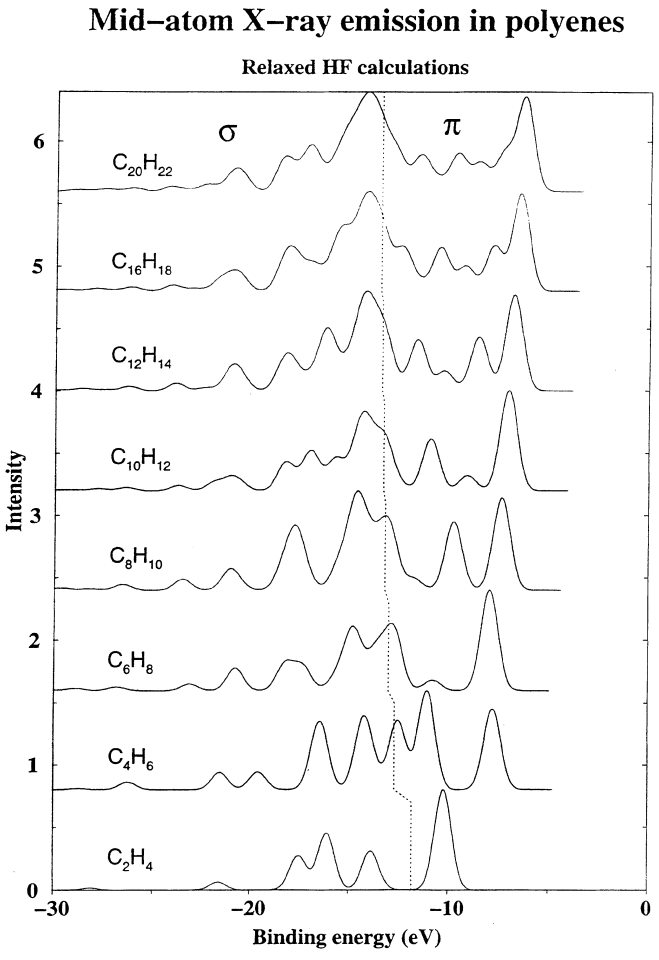

Fig. 7. Size dependence for X-ray emission spectra from the mid-atom in the $CH_2(C_2H_2)_nCH_2$, $n = 0, 1, 2, 3, 4, 5, 7, 9$ series. ΔSCF calculations. From Ref. [52]

The calculations show that the most important surface effect on the X-ray emission spectrum is a reordering of the outer 1π and 5σ derived bands and an addition of metal-CO binding states appearing weakly on the high energy side of the spectra. For the large clusters the calculations predict intensity for relaxation-induced X-ray transitions from the π^* band representing a local occupied part of the 2π–$3d$ adsorbate-substrate bond.

The different approximation levels (the one-center, frozen orbital and relaxed orbital levels) seem to relate to each other in an equal way for the chemisorbed system as well as for the free molecule (again with the exception of the screening π^* level). In particular, the validity of the one-center model is confirmed for surface XES. This is an important conclusion, since the great majority of XES investigations are analyzed by means of the frozen orbital one-center model, which provides the "interpretability" of the X-ray emission experiment in terms of electronic structure theory of the ground state molecule. The assignment (energy, intensity, symmetry) of the states due to the cluster-adsorbate bonding appearing with small intensities on the high energy side of the main spectrum corroborates the results obtained with angular resolved XES detection. A more problematic feature is the intensity of the $3d$-π^* level, which is close to the vacuum level for the larger clusters, and thus is situated above the Fermi level. A large cluster using full ΔSCF is necessary to describe the screening relaxation for the π^* level. It seems that the question as to how it is represented in the experimental spectrum remains to be resolved. Finally, concerning the initial or the final state rules, the simulations of the CO/Cu(100) system did not actually give clear preference for either of these two rules.

3.3 Shake-up spectra

In relation to other core photoelectron processes the molecular core electron shake-up phenomenon has been considered notoriously difficult to interpret and difficult to attribute any diagnostic capability. These facts have been ascribed to the unusually large role of electron correlation, and to the fact that, despite the fact that the core hole is localized, the shake-up process itself is non-local. A few recent studies with the STEX technique have brightened the picture somewhat; when the shake spectra are computed in the appropriately spin-coupled two-hole potentials taking account of the full intra-channel interaction close to the basis set limit, it is found that an orbital description may be successful in reproducing trends as well as specific features in the spectra. The full intra-channel, full basis set limits should thus constitute a suitable starting point for systematic improvements in terms of inter-channel coupling.

The convergence patterns indicate a complication-simplification trend with the size of the system, and actually lead to spectra that might be used as fingerprints, although the fingerprinting character is not as simple as in NEXAFS. A few systems, representing polymers, surface adsorbates and molecules with functional groups, have been studied with STEX resulting generally

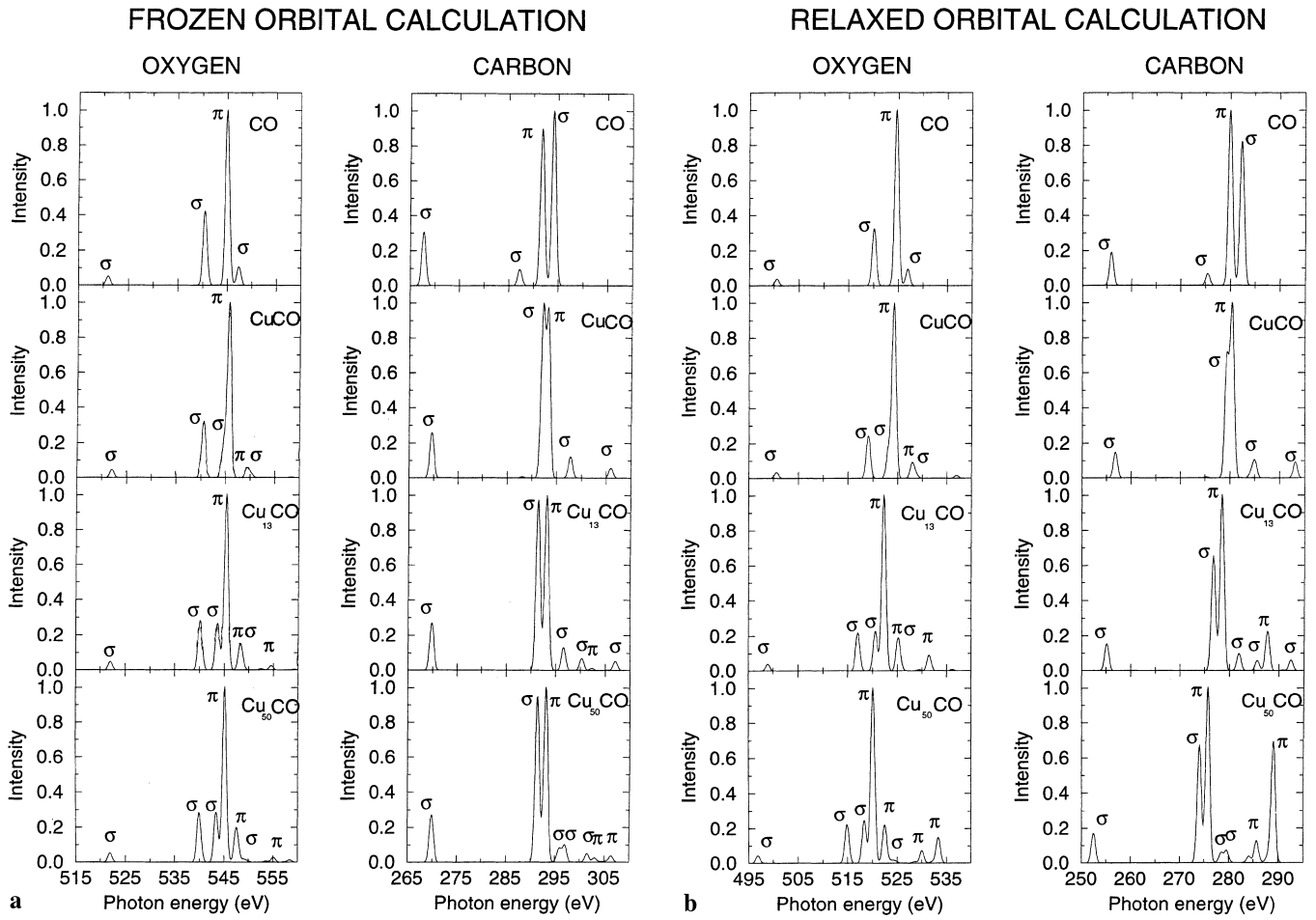

Fig. 8. a Oxygen and carbon XES spectra of Cu_NCO, $N = 0, 1, 13, 50$, obtained from frozen orbital (ground state) SCF calculations. (Frozen orbital core state energy is used). **b** Oxygen and carbon XES spectra of Cu_NCO, $N = 0, 1, 13, 50$, obtained from relaxed orbital (separate state) SCF calculations. From Ref. [58]

in a good account of experimental features obtained at the scale of resolution actually given by the experiment.

3.3.1 Free molecules

The application of STEX to free CO, which possesses a notoriously "difficult" shake-up spectrum, led to surprisingly good results. The low dominating π-π^* single excitation type transitions are well reproduced; the energy and intensity characters of most of the higher excitations, including those with some presumed double excitation character, still seem to be sufficiently well predicted to be used for assignments in terms of orbital excitations. With respect to other correlation schemes these results must be taken as indications of the importance of computing shake spectra at the full basis set limit and allowing for core-hole relaxation in the construction of the potential.

Other STEX applications refer to molecular aggregates which are of two types, one in which the same functional group is attached to a molecular backbone which is successively increased, and one using the same backbone but having different functional groups (substituents). For the former type the question arises how and whether the shake spectra converge to a pattern that can be used to fingerprint the functional group. A study on carbonyls attached to hydrocarbon backbones indicated that this indeed seems to be the case. Energy positions and intensities of the carbon and oxygen core-electron shake-up spectra showed rapidly converging and simplifying trends with respect to the size of the hydrocarbon chain. A relatively fast convergence of the spectra with respect to size was found, owing to the lowering of shake-off limits and the smearing of high-energy structures which act to simplify the spectra. In the long chain limit only one compound internal carbonyl and one charge transfer π-π^* band is predicted in the oxygen case, while two spin-split internal carbonyl bands are predicted for the carbon spectra.

This dominance of the LUMO level in organic shake spectra is typical, as are the strong charge transfer type contributions although the compounds might not be a charge-transfer species in the traditional sense. This stresses the importance of a non-local interpretation of shake-up spectra. Mono-substituted benzenes exemplify the second type of molecules with functional groups alluded to above. Also for these spectra one finds, through direct STEX calculations, that there are rather few (here π) levels actually involved in the formation of the shake spectra, with the LUMO level being the important un-

occupied level. As for NEXAFS, these compounds show a characteristic alternancy of energy and intensity with respect to site of excitation. Stronger substitution leads to stronger energy shift for the connected carbon, but actually to weaker energy shifts and intensity alternancy for the spectra of the unconnected carbons, making the spectrum more benzene-like and a good building block in shake-up studies.

The mono-substituted benzenes show excitation patterns that are characteristic for shake-up in general. Thus the low-energy features of the C_{1s} ring spectra are benzene-like with both levels (occupied and unoccupied) participating in the shake process being localized "on-site". The reverse substituent to ring transitions are present only at high energies, while for the substituent spectra the acceptor LUMO levels are still localized to the ring and the intensive low-energy features dominating the spectra are due to "off-site" transitions which are quite benzene-like. One thus finds that both the ring and the substituent shake spectra in these donor-type compounds are quite different from spectra of acceptor-type compounds, where the charge transfer transitions dominate, with on-site transitions emerging at high energies submerging the continuum. In surface-adsorbate acceptor spectra (see below) there is often also a reminiscence of the off-site (metallic) transitions, but then at very low energies, appearing as an asymmetrical broadening of the main core photoelectron lines [21, 59].

3.3.2 Polymers

As for NEXAFS, polyenes form a very suitable test ground for studying the site and size dependency of the shake spectra. The STEX technique seems to reproduce

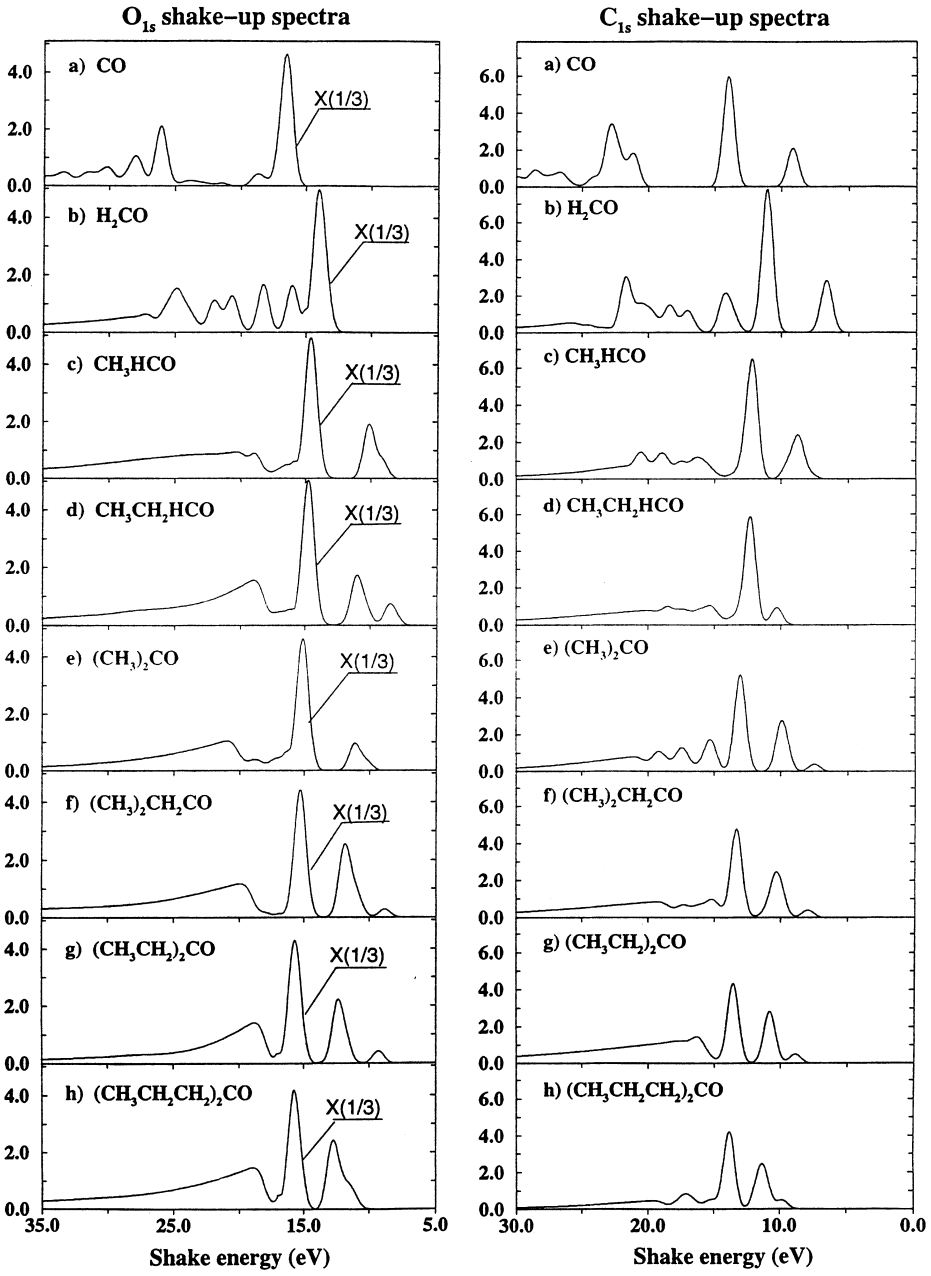

Fig. 9. Carbon and oxygen core electron shake spectra for carbonyl molecules. From Ref. [85]

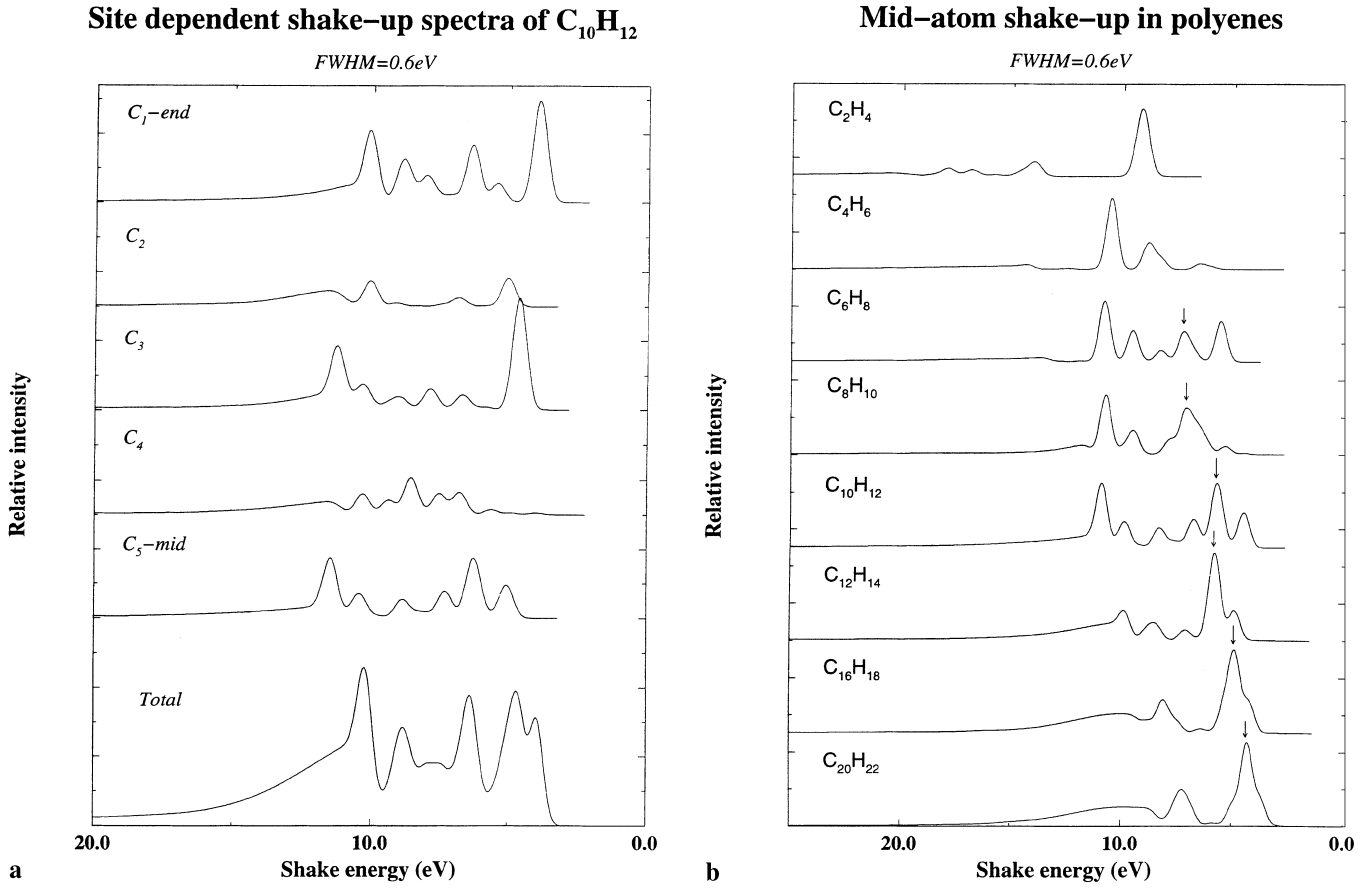

Fig. 10. **a** Site dependence of shake-up spectra of $C_{10}H_{12}$. **b** Size-dependent, mid-atom, shake-up spectra of polyenes. From Ref. [86]

the experimentally resolved spectra of the smaller members sufficiently well to justify such an analysis. The site dependence is found to be strongly alternant, which can be associated with a strong alternant localization of the LUMO level. Both end- and mid-atom spectra show a pattern of complication-simplification as the polyene chain grows longer, with polyenes of intermediate size showing intensity in regions where neither the monomer nor the long polyenes show intensity. The simplification results from the fact that rather few levels become involved, and that much detailed structure submerges into the continua of the different shake channels. An interesting aspect of these types of shake spectra is that they can be characterized both by initial (band formation) and final state (exciton formation) rules. This is because the shake energies follow the convergence of the band of (highest) occupied π orbitals, while intensities show quite stable excitonic character. It has been argued that, due to the more attractive potential, the effective core-valence interaction is stronger and therefore that conditions for excitations are more favorable than for NEXAFS. Thus STEX calculations predict excitonic behavior for shake-up but not for X-ray absorption of polyacetylene.

3.3.3 Surface adsorbates

Shake-up spectra of surface adsorbates show some salient features compared to the free molecular case, like characteristic lowering of the shake-up energies and strong increase of their intensities. These features are known to be very dependent on the strength of interaction between the surface and the adsorbate and have been proposed for use to characterize the interaction. Calculations of such spectra have been challenging for several reasons, and in particular the cluster convergence and the role of many-electron effects have been debated issues. For chemisorbed species, results of STEX calculations seem to conform with a three-fold division of the spectra; at a very low energy end, almost overlapping the main transitions, there is intense excitation with mainly cluster character; a few eV to the high energy side of the main peak one finds very intense low-lying charge back-transfer transitions, and a third high-energy region overlapping the continuum, characterized by intramolecular excitations that preserve the signatures of the corresponding transitions in the free molecule. The strong second region seems to be very dependent on the chemisorption strength. The orbitals responsible for these shake-up transitions can, through calculations, be assigned special bonding and anti-bonding characters, which, however, change quite drastically due the core-hole induced relaxation connected with the large shake intensities. A quite slow cluster convergence for a system like $COCu_N$ was predicted, e.g. the $COCu_{14}$ species only accounts for

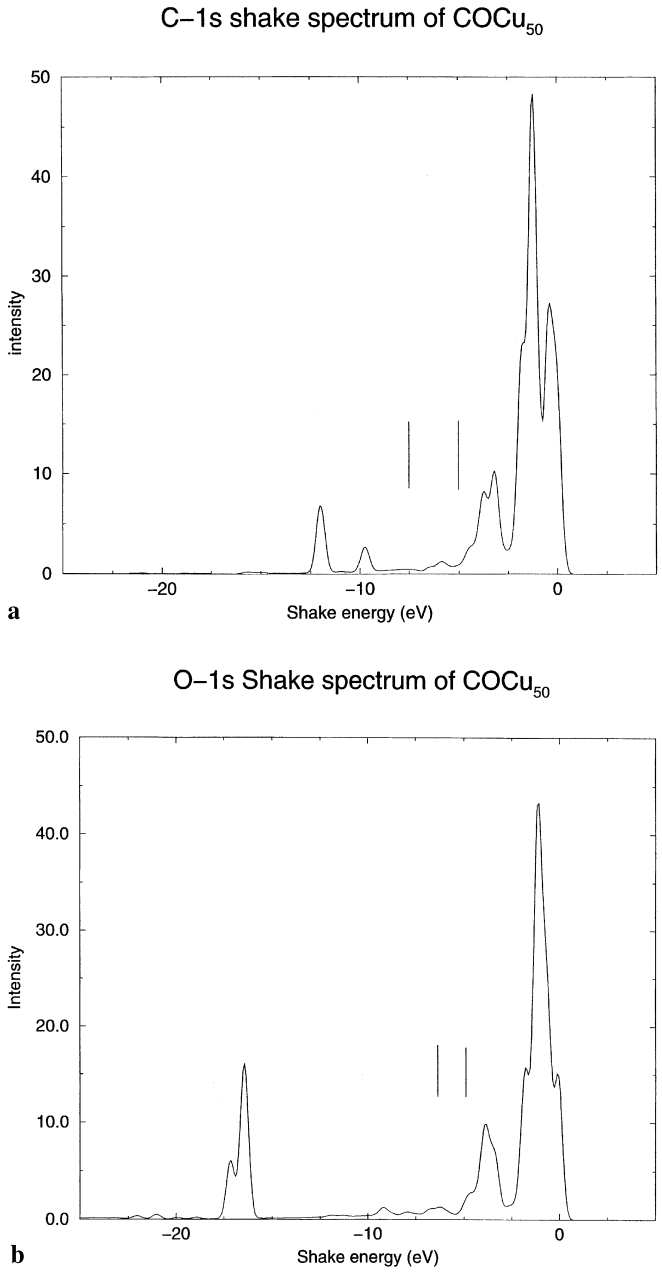

Fig. 11a, b. Core electron shake spectra for $COCu_{50}$ computed by STEX. **a** Carbon spectrum. **b** Oxygen spectrum. From Ref. [21]. The two bars indicate the onset of σ and π channel shake-off thresholds, respectively. The intensity is normalized to the intensity of the main state (not shown)

half the cluster induced shake-up/off intensity covered by $COCu_{50}$, and which can be a troublesome feature for cluster calculations.

3.4 Photoionization cross sections

Although ultraviolet photoelectron spectroscopy has been used quite extensively as a diagnostic tool for species of technological interest, such as polymers, polymer interfaces, and surface adsorbates [60–63], comparatively little theory development and computations have addressed the cross sections for photoionization of such extended systems. Most studies have focussed on the distribution and density of energy levels based on one-particle semi-empirical or Hartree-Fock approximations. The calculations of cross sections, partial and total, and the energy dependence of the cross sections have not been investigated to the same extent, probably much owing to the problem of computing continuum photoelectron functions in the anisotropic molecular potentials. The STEX technique, being both size-extensive and scalable, should be a viable candidate for calculations of such cross sections. It allows for an easy interpretation of the photo-process in terms of partial channels, which are indeed the experimentally relevant quantities. As in the shake-up analysis described above, a pragmatic approach is taken in that a comparison with highly resolved spectra of the smaller members of the oligomer series or by the free molecule in the surface adsorbate case is used to calibrate the method. Some prototype systems for polymers and "surface adsorbates" have been investigated by the STEX method as briefly reviewed below.

3.4.1 Free molecules

The STEX method has been used extensively for characterization of UPS spectra and photoionization cross sections of small free molecules (see, for example, review by Gallagher et al. [64]). As described in Sec. 2 it includes full intra-channel coupling but excludes inter-channel coupling. The interchannel coupling is not important for core photoionization, because of the large energy separation of the different core channels and of the core and valence channels. For inner valence levels the spectra are smeared out due to vibrational and dissociative broadening and due to configurational splitting [65, 66], and the independent channel (or independent particle) analysis should only be applied to the gross intensity distributions rather than to a state-by-state analysis. Outer valence levels are separated better in actual measurements and they are also described better by independent particle or quasi-particle pictures. A reasonable agreement is also obtained for the energy-dependent partial and total cross sections, except for the low energy region (below 20 eV), where the embedding of discrete states of closed channels into the continuum of open channels implies interactions that are not describable by STEX. In the STEX method one may thus obtain artificial discontinuities at the ionization potentials that may be caused by summing up cross sections from the independent

►

Fig. 12. A Energy-dependent partial photoionization cross sections of polyenes calculated by STEX. **a** C_2H_4 all channels, **b** $C_{10}H_{12}$ all π channels, **c** HOMO π channel for $C_{2n}H_{2(n+1)}, n = 1, 2, 3, 5, 8$, **d** LOMO π channel for $C_{2n}H_{2(n+1)}, n = 1, 2, 3, 5, 8$. The vertical *dotted-dashed* lines at 21.2 eV and 40.8 eV mark the He I and He II photon energy. **B** UPS spectra of polyenes $C_{2n}H_{2(n+1)}$ with $n = 1, 2, 3, 5$, calculated by STEX. **a** He I excitation, **b** He II excitation. From Ref. [68]

Energy dependent Partial cross section of polyenes

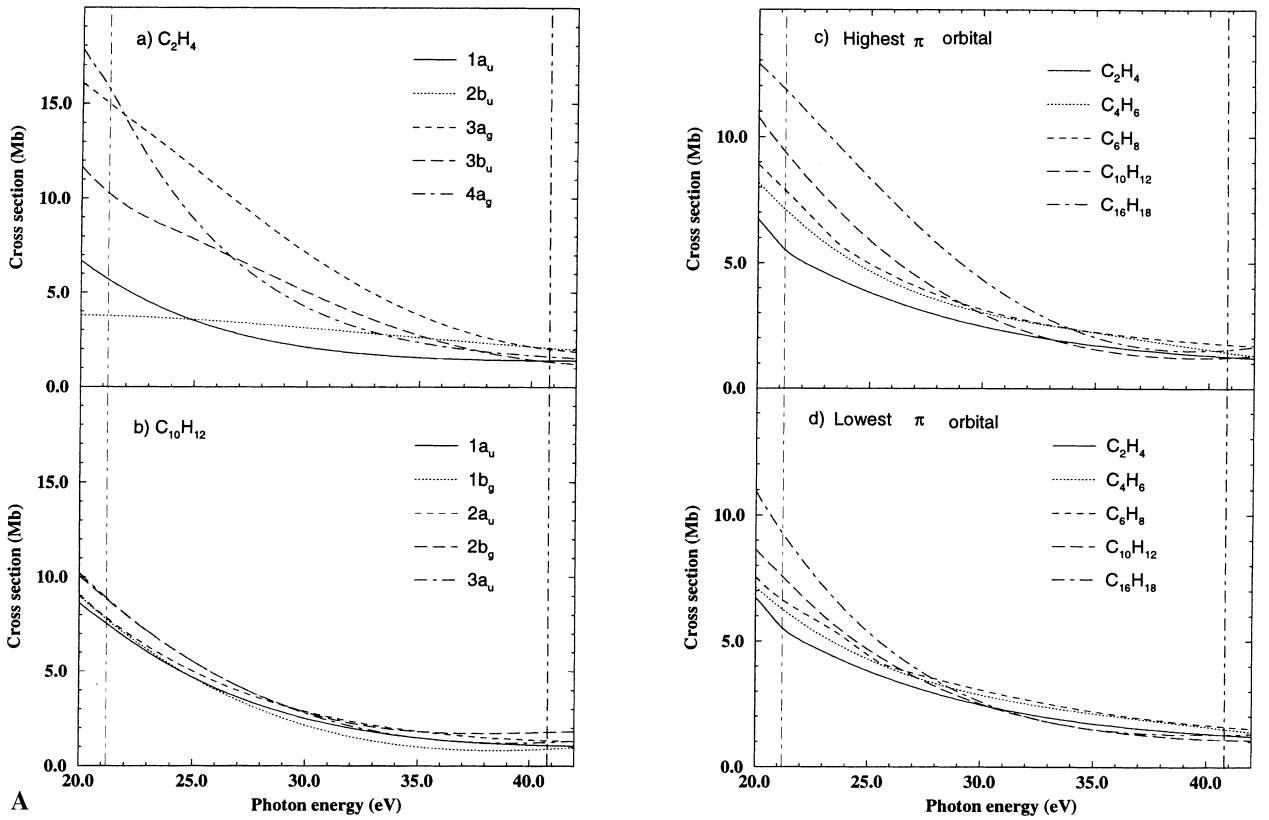

A

UV photoelectron spectra of polyenes

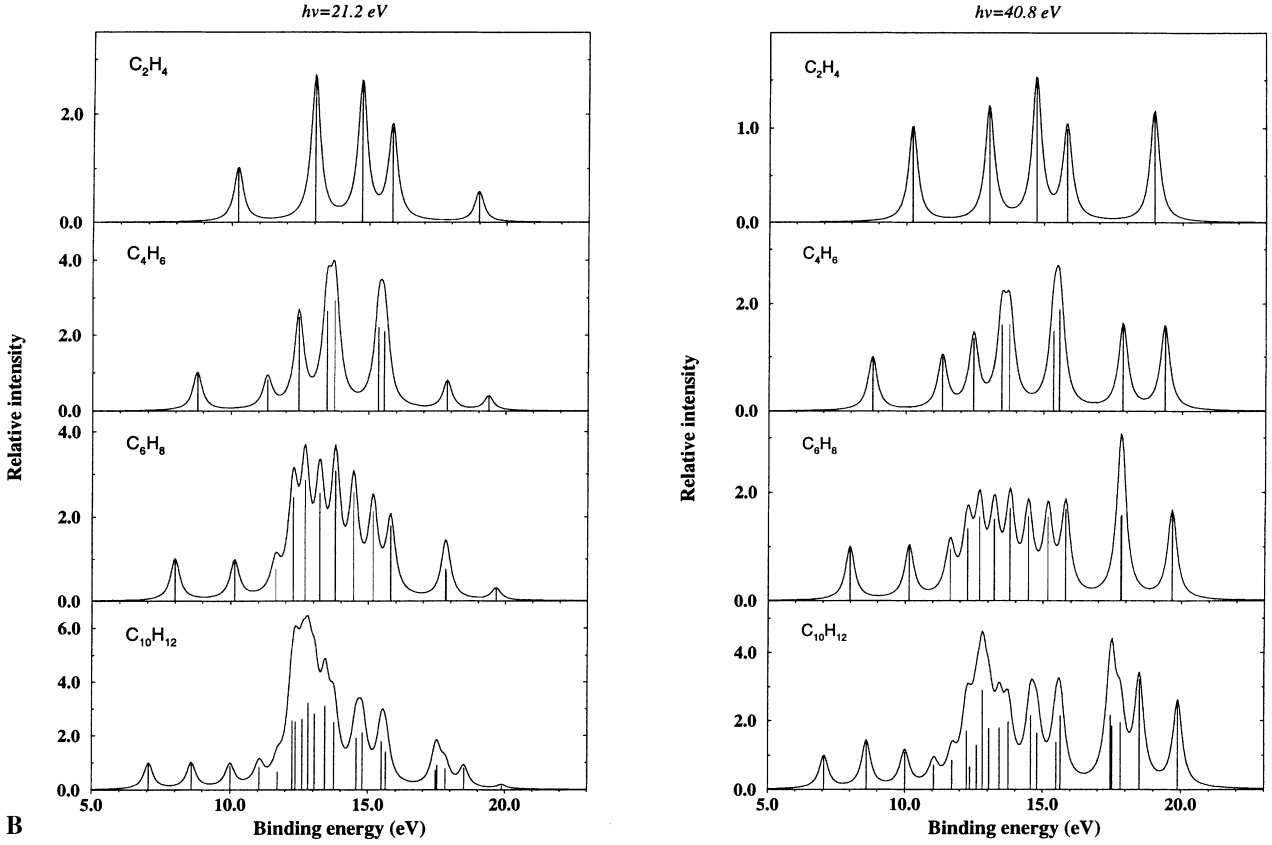

B

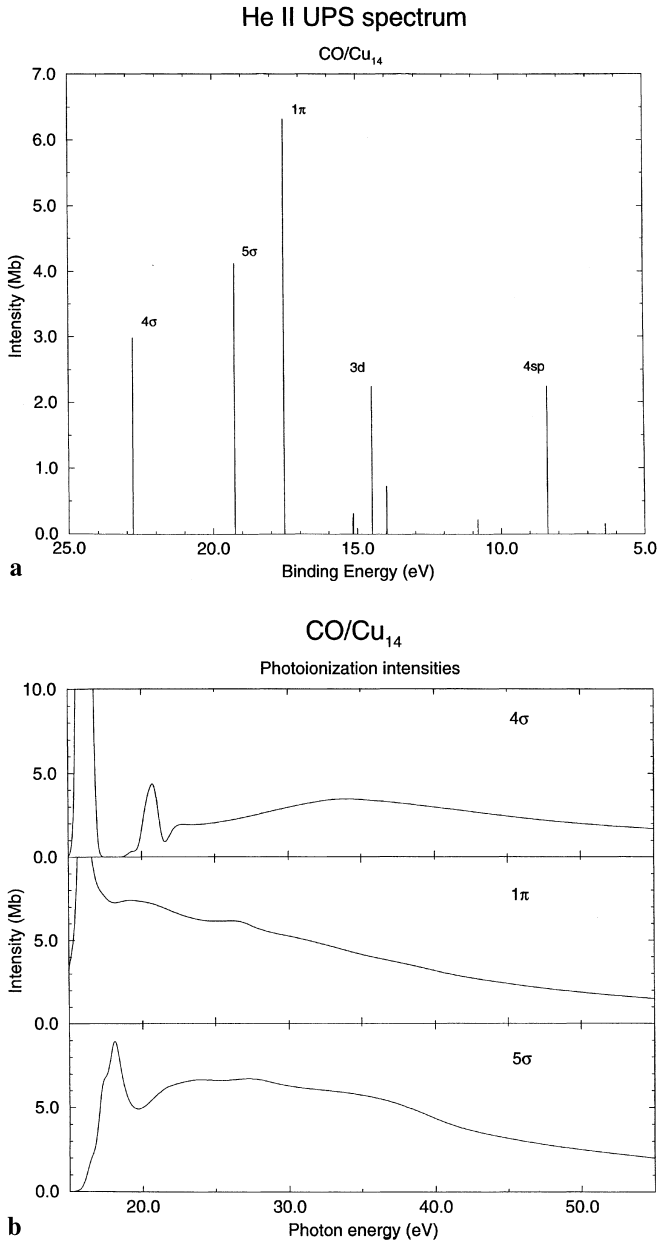

Fig. 13. Computed and He II UPS spectrum (**a**) and photoionization cross sections (**b**) (length gauge) for CO/Cu_{14}. From Ref. [67]

channels while the redistribution of intensity among partial channels due to the channel coupling is neglected.

The independent channel static-exchange method was employed in Ref. [67] to compute partial channel photoionization cross sections and photoelectron spectra in the ultraviolet energy region of the carbonyl systems CO and $Cr(CO)_6$ used as precursors for the CO/Cu_{14} cluster, which in turn models the CO/Cu(100) adsorbate (see Sect. 3.4.3). The dependences on photon energy, including He I and He II spectra, and on the particular ionization channel were then investigated. It was found that the method is indeed able to reproduce the essential trends and features of the spectra as well as the energy dependences of the cross sections for both CO and $Cr(CO)_6$. With the good general agreement with experimental data, assignment of the $Cr(CO)_6$ spectrum could be proposed. This also goes for the complex features in this spectrum due to CO outer valence 5σ and 1π orbitals interacting with the Cr $3d$ levels. The remarkable shape resonance in the 4σ channel is well reproduced for CO, and can also be traced, and enhanced, in $Cr(CO)_6$. The computed individual channel cross sections for $Cr(CO)_6$ show strong oscillations at low energies, which emerge as enhanced shape resonances introduced by a large potential barrier, as is known to be the case for highly coordinated, symmetrical compounds like $Cr(CO)_6$. By and large, the one-particle picture holds well for CO and $Cr(CO)_6$, although many-body contributions seemingly reduce the cross section at higher energies.

3.4.2 Polymers

As a first test of the STEX technique applied to larger oligomers, calculations were carried out for partial channel photoionization cross sections and photoelectron spectra of polyenes in the ultraviolet wavelength region. The dependences on molecular size, on photon energy and on the particular ionization channel were investigated in Ref. [68]. The polyenes serve both as a good model system for the evaluation of the photoionization cross sections with size, and as a prototype system for the role of doping on the electronic structures, in particular the introduction of states in the band gap. UV photoelectron spectroscopy has in fact been used as a diagnostic tool for such systems. A common assumption is that the π channels have equal photoionization cross sections, and that the spectra can be characterized in a simplified analysis by accounting only for the distribution (or density) of states, rather than their full ionization cross sections.

It was found in Ref. [68] that the channel dependence for cross sections at low (He I) photon energies is quite strong for the small species but diminishes as the molecular length is increased. The channel dependence also becomes weaker for higher photon energies. The energy dependence, which is strong in the He I region for all molecules/channels, is insignificant for He II excitation with the cross sections of all channels being close to each other. The cross sections are remarkably constant for the different π levels at any given photon energy. For the longer polyenes the convoluted spectra actually become determined mostly by the distribution of states rather than by the individual intensities. This is so because, with one or two exceptions, all cross sections within the π or σ groups of states are of similar magnitude. The investigation thus verified the assumption of constant π channel cross sections often made in the analysis of polymer UPS spectra. However, a similar analysis of ring systems (pristine, i.e. polyene chains connecting two phenyl rings) actually indicates that this assumption is not valid for those particular systems.

A problem encountered for valence photoionization of large species, which is not severe either for core excitations or for valence excitations in small molecules, is the handling of the augmentation basis set describing the photoelectron function. Due to the delocalization of the valence orbitals, large multi-centered basis sets are

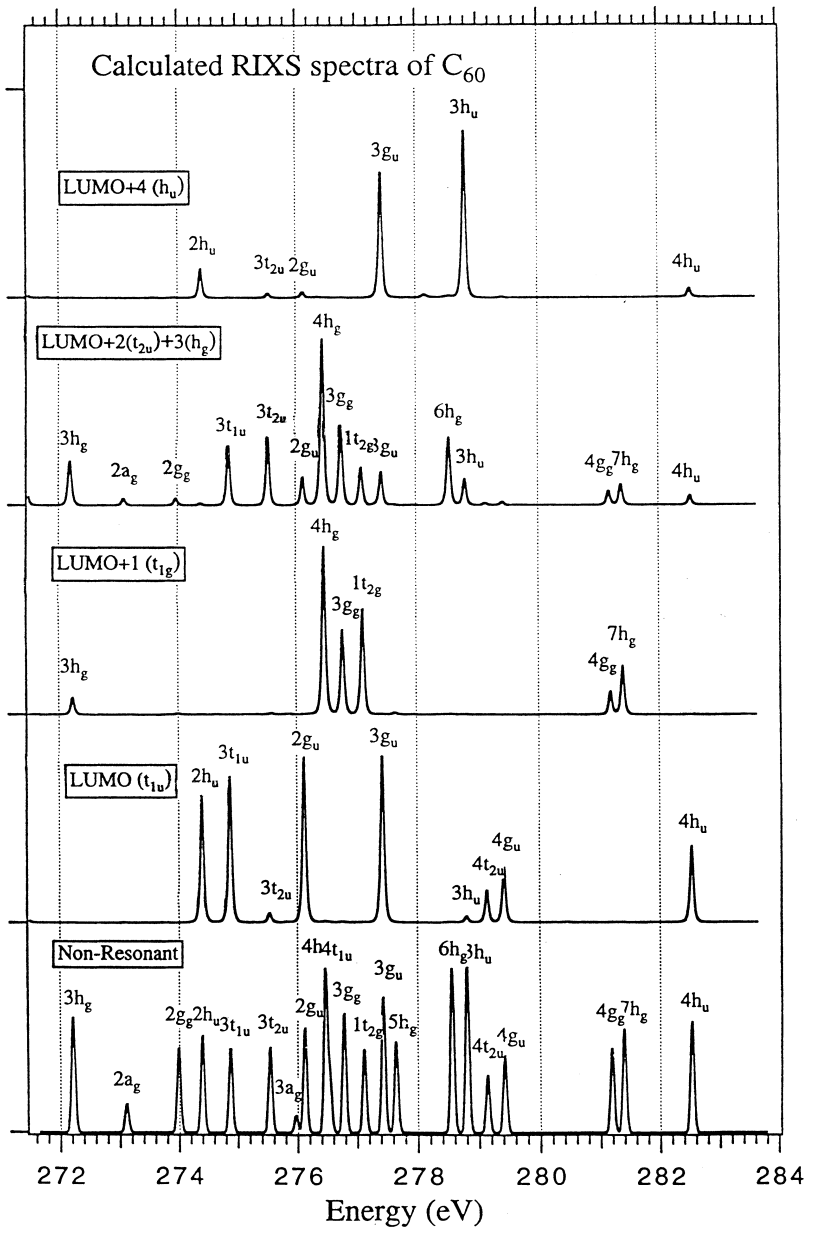

Fig. 14. Calculated non-resonant and resonant X-ray emission spectra of C_{60}. The absorption resonance levels are indicated in panels to the *left*. From Ref. [72]

required for the augmentation, thus strongly increasing the computational requirements. Due to this limitation the size of the systems reached in UPS cross section calculations can unfortunately not match what can be treated for the other spectroscopies discussed above.

3.4.3 Surface adsorbates

Since UV photoionization is a delocalized process, with signals representing the completely delocalized states, cluster modeling of surface UV photoionization is intrinsically more difficult than the treatment of core photoionization or valence photoionization of finite systems. Furthermore, taking into account the computational demands to describe the photoelectron function for large clusters, it is not evident that the cluster model can be successful. In this context it is also helpful to consider metallo-organic complexes, such as $Cr(CO)_6$ above as an intermediate between the free and the surface adsorbate systems with respect to the spectral properties investigated.

The UPS spectra of $COCu_{14}$ show salient differences with respect to the corresponding spectra of both CO and of $Cr(CO)_6$. Compared with CO the most apparent difference is evidently the addition of copper 3*d* and 4*sp* bands representing the enhancement of the CO/Cu(100) spectrum at a few eV's from the Fermi level. Another major difference to free CO is that the 5σ and 1π levels switch order in accordance with what is predicted for large clusters and for the full surface adsorbate system [58]. States due to the specific bonding between CO and the copper cluster are predicted with low intensity.

The simulation of the UPS spectrum of CO/Cu(100) by a limited cluster ($COCu_{14}$) seems to hold well concerning the organization of states, the gross spectral profiles and concerning the energy dependence of the

cross sections for the CO derived levels [69, 70]. The relative cross sections between the different parts of the spectra are assessed more qualitatively due to the involvement of several experimental parameters that are hard to simulate by a cluster model. The experimental comparison of channel cross sections is somewhat hampered by the strong angular dependency of UPS cross sections for a sample with fixed directions, and by the limited number of states given by the cluster model that should describe the metallic bands and the metallic photoionization cross section. Another difference with respect to oligomers of the organic systems is the limitation of one-particle (Koopmans) energies to characterize the spectra. While for the latter systems one general rescaling factor ($\simeq$1.3) can be used to grossly account for relaxation/correlation effects [45, 49, 71], the level energies in the surface adsorbate system are quite irregular with respect to relaxation/correlation; in the $COCu_{14}$ system some Cu3*d* derived states are subject to relaxation as strong as about 7–8 eV. Thus, corrections by ΔSCF and/or by correlated techniques (MCPF) were estimated in Ref. [67]; for an experimental comparison a correction with the work function is also relevant.

3.5 X-ray Raman spectra

The generation of resonant X-ray Raman scattering spectra is based on monochromatic X-ray excitation with small spectral widths (sometimes smaller than the lifetime broadening of the core-excited states) and on the ability to continuously tune the incoming X-ray frequencies near the ionization threshold. Using these techniques one obtains X-ray fluorescence spectra that are sensitively dependent on the frequency and spectral shape of the exciting radiation. For smaller species they have enabled the study of several "Raman" effects in the X-ray region, such as resonance narrowing below the lifetime width and linear dispersions of the resonant inelastic X-ray scattering. For somewhat larger species it is probably the symmetry and polarization selectivity character of the spectra that become most relevant as structural tools.

Simulations have been indispensable to establish how the symmetry and polarization selectivity is manifested in actual recordings of Raman spectra. The C_{60} molecule with its high icosahedral symmetry (I_h) constitutes perhaps the most conspicuous test case of them all.

Figure 14 shows the Raman spectra of C_{60} from direct SCF simulations using canonical Hartree-Fock theory [72]. The general symmetry handling of the DISCO program greatly facilitates both the simulation as such and the output analysis for a point group as high as I_h. The different panels in Fig. 14 correspond to Raman spectra referring to different resonantly excited core levels; the lowest panel shows the non-resonant

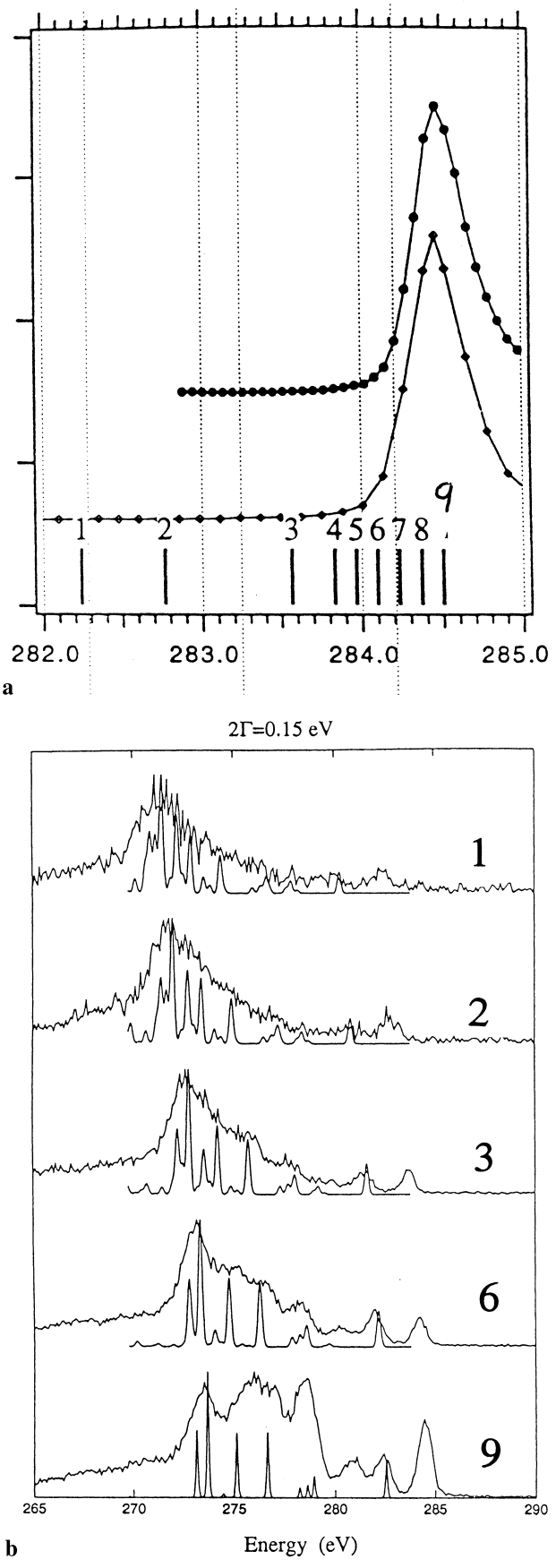

Fig. 15. a Lowest NEXAFS band of C_{60}. **b** Experimental and simulated resonant X-ray Raman spectra of C_{60} corresponding to the detuned excitation energies. From Ref. [72]

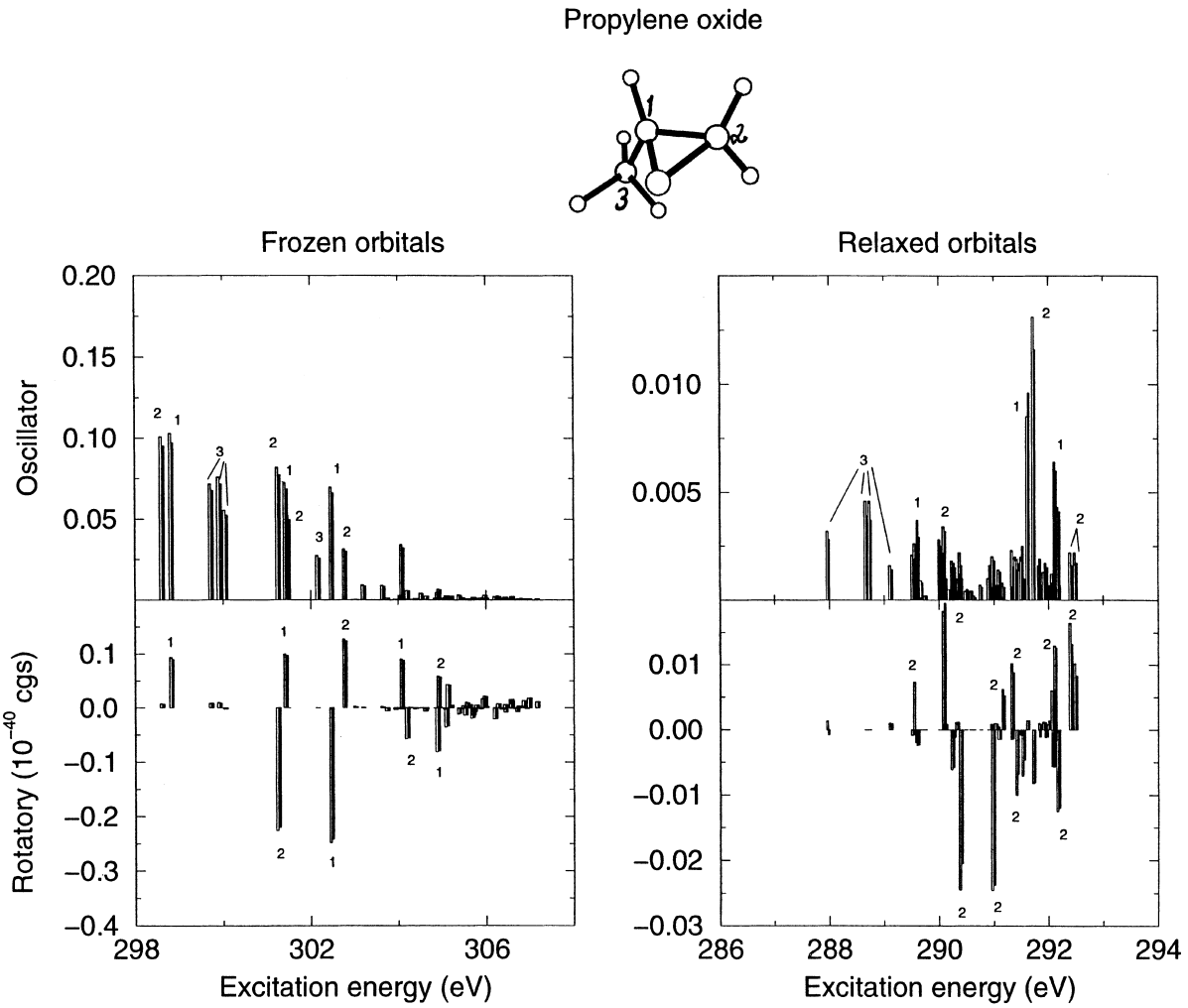

Fig. 16. Oscillator and rotatory strengths of carbon core excited states of propylene oxide below the highest ionization threshold, calculated using frozen and relaxed orbitals in the length (*open bars*) and velocity (*filled bars*) gauge. The labels indicate the localization of the carbon core orbital involved in the excitation (see *top panel*). From Ref. [12]

spectrum. It is clear from the figure that the Raman spectra of C_{60}, as computed from the scattering tensors in the full point goup, are highly symmetry selective and therefore also very dependent on the frequency of the exciting X-ray photons. Actually it has been shown that, with the possibility of using either linearly or circularly polarized radiation, all electronic states for molecules of any symmetry can in principle be assigned through X-ray Raman spectra [73]. The comparison with experimental spectra indicates that the symmetry selectivity is less prominent than predicted from pure electronic structure theory. For higher core-excited resonances this can be explained by the closeness of states and "tail excitation"; however, as the lowest panel of the figure indicates, the spectrum referring to the LUMO resonant X-ray Raman spectrum of C_{60} actually shows features not explained by the symmetry selectivity of the electronic I_h group. One explanation could be the formation of excitons, which is neglected in canonical Hartree-Fock theory. Such a character is obvious for small species with large core-valence interaction, while for larger species, with reduced interaction, the excitonic character becomes very system dependent. Another explanation refers to effects due to vibronic coupling. As seen in Fig. 15, the Raman spectra pertaining to detuned frequencies in the "band gap" seem to restore the symmetry selectivity of the spectroscopy. In fact, as has recently been demonstrated, the vibronic coupling-induced symmetry breaking is strongly dynamic, and is quenched by detuning the frequency away from the resonance [74]. Taking this fact into account, direct SCF canonical Hartree-Fock theory seems to be a good method for studying X-ray Raman spectra of species like C_{60} and other fullerenes [50].

3.6 Natural circular dichroism

As a final example of applications with the direct STEX/direct SCF technique we briefly comment on some recent applications to circular dichroism (CD), in particular natural X-ray CD in the absorption, emission and Raman modes. Dichroism is a property of "chiral" molecules with distinguishable mirror images, and which thus interact

differently with left or right circularly polarized light. The phenomenon has long been studied in the optical region [75], experimentally as well as the oretically, and has found applications in a wide variety of systems, for instance in organic molecules of biological interest.

The development of sources for tunable synchrotron radiation with circular polarization has created interest in CD effects also in the X-ray region. Most efforts in this direction have been devoted to magnetic field induced circular dichroism (MCD), but natural dichroism is also of interest since it can add a new selective feature to NEXAFS and possibly also to XES spectroscopy, which are both known to be element and chemical selective for "ordinary" X-ray radiation. As for ordinary X-ray spectra, the role of relaxation might be crucial, both for relaxing the "chiral" surrounding and for polarizing the core orbital. Similar to the case of ordinary spectra, the STEX method has an advantage over the commonly used RPA method (although being a strict approximation of it, see Sect. 2), in that it easily takes care of relaxation effects. As described in Sect. 2, STEX completely neglects interchannel coupling contributions to CD; it can, however, be safely assumed that the interchannel coupling is more important than relaxation for valence excitations, while the reverse is true for core excitations, something actually confirmed by the studies reviewed here. In fact, we find the RPA values to be quite close to STEX results using frozen orbital potentials.

Studies using the STEX technique have been performed for X-ray rotatory strengths and CD intensities in organic molecules, using twisted ethylene as a test case and propylene oxide and *trans*-1-2 dimethylcyclopropane as possible candidates for experimental measurements [12]. These molecules have also served as standard cases for test calculations of rotatory strengths in the optical region [75]. The results obtained from STEX calculations for propylene oxide are recapitulated in Fig. 16 and we notice, as expected, large deviations between relaxed and frozen excitation energies, which also brings about an energy reordering of the excitations. Using augmented basis sets there is in general very good agreement between length and velocity gauge results for both oscillator and rotatory strengths. We also observe large variations of both oscillator and rotatory strengths going from frozen to relaxed orbitals. As also observed for *trans*-1,2-dimethylcyclopropane, there is a strong reduction of rotatory intensity, about one order of magnitude, with an anisotropy ratio g ending up in the range of 10^{-4}–10^{-3}. This seems anyway to be in the range reachable by the present, or soon to be available, experimental equipment at synchrotron radiation laboratories [76].

Another interesting effect in X-ray CD spectra is illustrated by Fig. 16, namely the chemical shifts. First, one notes from the figure that the discrete region of the total NEXAFS spectrum receives contributions from excitations of all three C-1*s* orbitals. The distribution of rotatory strength appears quite different; the excitations involving the methyl carbon atom, in the low energy region of the spectrum, have negligible g values and the discrete excited states that show a dominant CD are those belonging to the methylene channel.

A corresponding, direct ΔSCF investigation, on the *trans*-1-2 dimethylcyclopropane and propylene oxide molecules was recently also conducted for natural X-ray CD in the non-resonant emission mode [77]. As in the absorption mode, emission CD was indeed found to be both chemically and element dependent, while the calculations showed that electronic relaxation is much less crucial than in X-ray absorption. The CD effect is much larger for systems with shallow core orbitals, e.g. larger for carbon than for oxygen species, due to the large contribution of core orbital polarization. A conclusion from the work of Ref. [77] was that the natural CD effect should also be observable in X-ray emission.

Finally, chirality, or rather rotatory intensity differences, has also been predicted with the direct SCF technique for the X-ray Raman experiment [78]. Applications of a new formalism for randomly oriented molecules with direct SCF canonical Hartree-Fock theory calculations indicate very strong effects for C_{60} and other molecules containing elements of symmetry. These effects can be associated with the fact that the pure electric dipole contribution to the CD can be very large for such molecules, actually about one order of magnitude larger than the magnetic dipole contributions. This strong CD can only be described by a one-step model for X-ray Raman scattering, while in the two-step model the electric CD contribution is identically zero. It is intimately connected to the molecular point group symmetry and to channel interference, and, in contrast to optical CD, it will be preferentially observed for "achiral" molecules [78].

4 Conclusion

In the present work we have discussed the unifying aspects of calculations of electronic spectra by means of the direct SCF direct static-exchange method. Free molecules, finite polymers, and surface adsorbates have been employed as demonstration samples for this purpose. The usefulness of the direct SCF direct static-exchange method is obvious from the reviewed applications which now cover a representative cross section of spectroscopies and of chemically and physically interesting problems. Although the actual implementation of the method is quite well advanced, one can foresee developments of several aspects: of the basic methodology as well as of a wide-scope of systems and phenomena that can be investigated. It is our hope that the present review has provided new ideas in that direction.

5 Epilogue

The project reviewed in this work was initiated whilst two of the present authors were at the Minnesota Supercomputer Institute in the fall of 1993. On that occasion, just as during several previous visits that all four authors made to the institute, we enjoyed the generosity and friendly exchange of ideas with Jan Almlöf and the brilliance which always characterized his

conversations regarding matters of theoretical chemistry. It was with great sadness that we received the news that he passed away. We have lost a dear colleague and an exemplary individual with an extraordinary ability to combine scientific success with honesty and friendship.

Acknowledgements. This work was supported by grants from the Swedish and Italian Science Research Councils, NFR and CNR.

References

1. Almlöf JE, Faegri K Jr, Korsell K (1982) J Comput Chem 3:385
2. Helgaker T, Jensen HJAa, Jørgensen P, Koch H, Olsen J, Ågren H, Andersen T, Bak KL, Bakken V, Christiansen O, Dahle P, Dalskov EK, Enevoldsen T, Halkier A, Heiberg H, Jonsson D, Kirpekar S, Kobayashi R, de Meras AS, Mikkelsen KV, Norman P, Packer MJ, Ruud K, Saue T, Taylor PR, Vahtras O, DALTON, an ab initio electronic structure program
3. Frisch MJ, Trucks GW, Schlegel HB, Gill PMW, Johnson BG, Robb MA, Cheeseman JR, Keith TA, Petersson GA, Montgomery JA, Raghavachari K, Al-Laham MA, Zakrzewski VG, Ortiz JV, Foresman JB, Cioslowski J, Stefanov BR, Nanayakkara A, Challacombe M, Peng CY, Ayala PY, Chen W, Wong MW, Andres JL, Replogle ES, Gomperts R, Martin RL, Fox DJ, Binkley JS, Defrees DJ, Baker J, Stewart JP, Head-Gordon M, Gonzales C, Pople JA (1995) GAUSSIAN 94 (revision A.1). Gaussian, Inc., Pittsburgh, Pa
4. Feyereisen M, Nichols J, Oddershede J, Simons J (1992) J Chem Phys 96:2978
5. Ågren H, Koch H, Vahtras O, Jørgensen P, Helgaker T (1993) J Chem Phys 98:6417
6. Ågren H, Carravetta V, Vahtras O, Pettersson LGM (1994) Chem Phys Lett 222:75
7. Koch H, Ågren H, Jørgensen P, Helgaker T, Jensen HJAa (1993) Chem Phys 172:13
8. Norman P, Jonsson D, Vahtras O, Ågren H (1995) Chem Phys Lett 242:7
9. Dunning TH, Mckoy V, (1967) J Chem Phys 47:1735
10. Jørgensen P, Jensen HJAa, Olsen J (1988) J Chem Phys 89:3654,
11. Carravetta V, Luo Y, Ågren H (1993) Chem Phys 174:141
12. Carravetta V, Vahtras O, Ågren H, Plachkevytch O (1997) Chem Phys Lett 00:000
13. Ågren H, Carravetta V, Pettersson LGM, Vahtras O (1995) Physica B, 208:477
14. Langhoff P W (1979) In: Rescigno TN, McKoy BV, Schneider B (eds) Electron molecule and photon molecule collisions. Plenum, New York, p 183
15. Langhoff PW (1980) In: Dalton BJ, Grimes SM, Vary JP, Williams SA (eds) Theory and application of moment methods in many-fermion systems. Plenum, New York, p 191
16. Amos AT, Hall CG (1961) Proc R Soc A 263:483
17. Malmqvist PÅ (1986) Int J Quantum Chem 30:479
18. Ågren H, Carravetta V (1987) J Chem Phys 87:370
19. Ågren H, Carravetta V (1992) Int J Quantum Chem 42:685
20. Nordfors D, Nilsson A, Svensson S, Mårtensson N, Gelius U, Ågren H (1991) J Electron Spectrosc Rel Phenom 56:117
21. Ågren H, Carravetta V, Pettersson LGM, Vahtras O (1996) Phys Rev B 53:16074
22. St-Amant A, Salahub DR (1990) Chem Phys Lett 169:387
23. Salahub DR, Fournier R, Mlynarski P, Papai I, St-Amant A, Ushio J (1991) In: Labanowski J, Andzelm J, (eds) Density functional methods in chemistry, Springer, New York Berlin Heidelberg, p 77; St-Amant A (1992) Ph.D. thesis, Université de Montréal. The present version of the program has been substantially modified by L.G.M. Pettersson
24. Tatewaki H, Huzinaga S. (1979) J Chem Phys 71: 4339
25. Mattsson A, Panas I, Siegbahn P, Wahlgren U, Åkeby H (1987) Phys Rev B 36:7389
26. Wahlgren U, Siegbahn PEM, (1991) In: Salahub D (ed) Metal-ligand interactions: from atoms, to clusters, to surfaces. Kluwer, Dordrecht, p 199
27. Naved de Brito A, Correia N, Svensson S, Ågren H (1991) J Chem Phys 95:2965.
28. Eberhardt W, Rubensson JE, Randall KJ, Feldhaus J, Kilcoyne ALD, Bradshaw AM, Xu Z, Johnson PD, Ma Y (1992) Phys Scr T41:143
29. Ågren H, Yang L, Carravetta V, Pettersson LGM (1996) Chem Phys Lett 259:21
30. Stöhr J (1992) NEXAFS spectroscopy. Springer, Berlin Heidelberg, New York
31. Outka DA, Stöhr J, Madix RJ, Rotermund HH, Hermsmeier B, Solomon (1987) J Surf Sci 185:53.
32. Pettersson LGM, Ågren H, Schürmann BL, Lippitz A, Unger Wes (1997) Int J Quant Chem 63:749
33. Ågren H, Carravetta V, Vahtras O, Pettersson LGM (1995) Phys Rev B 51:17848
34. Ågren H, Carravetta V, Vahtras O (1995) Chem Phys 195:47
35. Carravetta V, Ågren H, Pettersson LGM, Vahtras O (1995) J Chem Phys 102:5589
36. Gel'muhanov F, Ågren H. (1995) J Chem Phys 103:6848
37. Brühwiler P, Maxwell AJ, Puglia C, Nilsson A, Andersson S, Mårtensson N (1995) Phys Rev Lett 74:614
38. Brühwiler P, Kuiper P, Eriksson O, Ahuja R, Svensson S (1996) Phys Rev Lett 76:1761
39. Yokoyama T, Seki K, Morisada I, Edamatsu K, Ohta T (1990) Phys Scr 41:189
40. Pettersson LGM, Ågren H, Vahtras O, Carravetta V (1995) J. Chem Phys 103:8713
41. Pettersson LGM, Ågren H, Vahtras O, Carravetta V (1996) Surf Sci 365:581
42. Hermann K, Witko M, Pettersson LGM, Siegbahn P (1993) J Chem Phys 99:610
43. Panas I, Schüle J, Siegbahn PEM, Wahlgren U (1988) Chem Phys Lett 149:265
44. Yang L, Ågren H, Pettersson LGM, Carravetta V (1997) J Electron Spectrosc Rel Phenom 82:209
45. Manne R (1970) J Chem Phys 52:5733
46. Ågren H, Nordgren J (1981) Theor Chim Acta 58:111
47. Ågren H, Arneberg R (1983) Phys Scr 28:80
48. Nordgren J, Ågren H (1984) Comments At Mol Phys 14:203
49. Guo JH, Luo Y, Vahtras O, Skytt P, Wassdahl N, Ågren H, Nordgren J (1994) Chem Phys Lett 227:98
50. Guo JH, Skytt P, Wassdahl N, Nordgren J, Luo Y, Vahtras O, Ågren H (1995) Chem Phys Lett 235:152
51. Gel'mukhanov F, Ågren H (1995) J Phys B: At Mol Phys 28:3699
52. Gelmukhanov F, Yang L, Ågren H (1996) J Chem Phys 105:5224
53. Luo Y, Liegener C, Ågren H (1995) Chem Phys. Lett., 233:123
54. Wassdahl N, Nilsson A, Wiell T, Tillborg H, Duda LC, Guo JH, Mårtensson N, Nordgren J, Andersen JN, Nyholm R (1994) Phys Rev Lett 69:812
55. Wiell T, Tillborg H, Nilsson A, Wassdahl N, Mårtensson N, Nordgren J (1994) Surf Sci Lett 304:L541
56. Nilsson A, Bennich P, Wiell T, Wassdahl N, Mårtensson N, Nordgren J, Björneholm O, Stöhr J (1995) Phys Rev B 51:10244
57. Ågren H, Flores-Riveros A, Jensen HJAa (1989) Phys Scr 40:745
58. Carravetta V, Pettersson LGM, Ågren H, Vahtras O (1996) Surf Sci 369:146
59. Tillborg H, Nilsson A, Mårtensson N (1993) J Electron Spectrosc Rel Phenom 62:73
60. Salaneck WR (1986) In: Skotheim TA (ed) Handbook of conducting polymers, vol II. Marcel Dekker, New York, 1986
61. Fahlman M, Lögdlund M, Stafström S, Salaneck WR, Fried RH, Burn PL, Holmes AB, Kaeriyama K, Sonoda Y, Lhost O, Meyers F, Bredas JL (1995) Macromolecules 28:1959
62. Fahlman M, Beljonne D, Lögdlund M, Friend RH, Burn PL, Holmes AB, Bredas JL, Salaneck WR (1995) Chem Phys Lett 214:327

63. Tillborg H, Nilsson A, Hernäs B, Mårtensson N, Palmer RE (1993) Surf Sci 295:1
64. M.C. Gallagher, M.S. Fgfield, J.P. Cowin and S.A. Joyce (1995) Surf. Sci. 339, 1909
65. Desjardins SJ, Bagawan ADO, Liu ZF, Tan KH, Wang Y, Davidson ER (1995) J Chem Phys 103:6385
66. Cederbaum LS, Domcke W, Schirmer J, von Niessen W (1986) Adv Chem Phys 65:115
67. Pascual J-L, Pettersson LGM, Ågren H. (1997) Phys. Rev. B. (in press)
68. Carravetta V, Yang L, Ågren H. (1997) Phys Rev B 000:00
69. Paolucci G, Surman M, Prince KC, Sorba L, Bradshaw AM, McConville CF, Woodruff DP (1986) Phys Rev B 34:1340
70. Heskett D, Strathy I, Plummer EW, de Paola RA (1985) Phys Rev B 32:6222
71. Orti E, Brédas J-L (1988) J Chem Phys 89:1009
72. Luo Y, Ågren H, Guo J-H, Skytt P, Wassdahl N, Nordgren J (1995) Phys Rev A 52:14479
73. Luo Y, Ågren H, Gelmukhanov FK (1994) J Phys B: At Mol Phys 27:4169
74. Skytt P, Glans P, Guo JH, Gunnelin K, Såthe C, Nordgren J, Gel'mukhanov FKh, Cesar A, Ågren H (1997) Phys Rev Lett 55:134
75. Hansen AaE, Bouman TD (1980) Adv Chem Phys 44:545
76. Duda LC, Kuiper P, Mancini DC, Englund CJ, Nordgren J (1996) Nucl Instrum Methods A376:291
77. Vahtras O, Ågren H, Carravetta V (1997) J Phys B: At Mol Phys 00:000
78. Luo Y, Vahtras O, Gel'mukhanov F, Ågren H (1997) Phys Rev A 55:000
79. Hitchcock AP, Brion CE (1978) J Electron Spectrosc Rel Phenom 13:193
80. Ågren H, Arneberg R (1984) Phys Scr 30:55
81. Iwata S, Kosugi N, Nomura O (1978) Jpn J Appl Phys 17: 105
82. Kay RB, Ph. E. van der Leeuw, van der Wiel MJ (1977) J Phys B: At Mol Phys 10:2513
83. Hitchcock AP, Pocock M, Brion CE, Banna MS, Frost DC, MacDowell CA, Wallbank B (1978) J Electron Spectrosc Re Phenom 13:345
84. Ziegler C, Schedel-Niedrig T, Beamson G, Clark DT, Salaneck WR, Sotobayashi H, Bradshaw AM (1994) Langmuir, 10:4399
85. Yang L, Ågren H (1996) J Mol Struc (THEOCHEM) 388: 221
86. Yang L, Ågren H (1996) Phys Rev B 54:13649